Wiley Series in Biotechnology and Bioengineering
Anurag S. Rathore, Series Editor

Preparative Chromatography for Separation of Proteins

EDITED BY
Arne Staby • Anurag S. Rathore • Satinder Ahuja

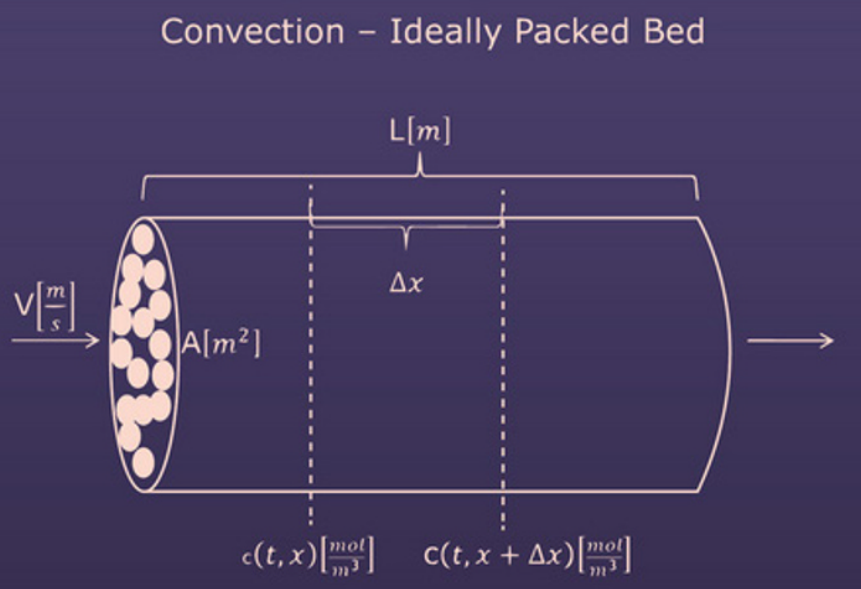

In - Out = Accumulated

WILEY

Preparative Chromatography for Separation of Proteins

Wiley Series in Biotechnology and Bioengineering

Significant advancements in the fields of biology, chemistry, and related disciplines have led to a barrage of major accomplishments in the field of biotechnology. **Wiley Series in Biotechnology and Bioengineering** focuses on showcasing these advances in the form of timely, cutting-edge textbooks and reference books that provide a thorough treatment of each respective topic.

Topics of interest to this series include, but are not limited to, protein expression and processing; nanotechnology; molecular engineering and computational biology; environmental sciences; food biotechnology, genomics, proteomics and metabolomics; large-scale manufacturing and commercialization of human therapeutics; biomaterials and biosensors; and regenerative medicine. We expect these publications to be of significant interest to the practitioners both in academia and industry. Authors and editors were carefully selected for their recognized expertise and their contributions to the various and far-reaching fields of biotechnology.

Preparative Chromatography for Separation of Proteins
by Arne Staby, Anurag S. Rathore, Satinder (Sut) Ahuja

Vaccine Development and Manufacturing
by Emily P. Wen (Editor), Ronald Ellis (Editor), Narahari S. Pujar (Editor)

Risk Management Applications in Pharmaceutical and Biopharmaceutical Manufacturing
by Hamid Mollah (Editor), Harold Baseman (Editor), Mike Long (Editor)

Emerging Cancer Therapy: Microbial Approaches and Biotechnological Tools
by Arsenio Fialho (Editor), Ananda Chakrabarty (Editor)

Quality by Design for Biopharmaceuticals: Principles and Case Studies
by Anurag S. Rathore (Editor), Rohin Mhatre (Editor)

Preparative Chromatography for Separation of Proteins

Edited by
Arne Staby, Anurag S. Rathore,
and Satinder Ahuja

WILEY

Published by John Wiley & Sons, Inc., Hoboken, New Jersey

Published simultaneously in Canada

For general information on our other products and services or for technical support, please contact our Customer Care Department within the United States at (800) 762-2974, outside the United States at (317) 572-3993 or fax (317) 572-4002.

Wiley also publishes its books in a variety of electronic formats. Some content that appears in print may not be available in electronic formats. For more information about Wiley products, visit our web site at www.wiley.com.

Library of Congress Cataloging-in-Publication Data:

Names: Staby, Arne, 1964– editor. | Rathore, Anurag S. (Anurag Singh), 1973– editor. | Ahuja, Satinder, 1933– editor.
Title: Preparative chromatography for separation of proteins / edited by Arne Staby, Anurag S. Rathore, Satinder Ahuja.
Description: Hoboken, New Jersey : John Wiley & Sons Inc., [2017] | Series: Wiley series in biotechnology and bioengineering | Includes bibliographical references and index.
Identifiers: LCCN 2016042817 | ISBN 9781119031109 (hardback) | ISBN 9781119031154 (epub)
Subjects: LCSH: Chromatographic analysis. | Separation (Technology) | BISAC: TECHNOLOGY & ENGINEERING / Chemical & Biochemical. | SCIENCE / Life Sciences / Biochemistry. | SCIENCE / Chemistry / Analytic.
Classification: LCC QD272.C4 P75 2017 | DDC 572/.64028–dc23
LC record available at https://lccn.loc.gov/2016042817

Set in 10/12pt Warnock by SPi Global, Pondicherry, India

Cover Design: Wiley
Cover Image Credit: Courtesy of L. Sejergaard, H. Ahmadian, T.B. Hansen, A. Staby, and E.B. Hansen.

Printed in the United States of America

10 9 8 7 6 5 4 3 2 1

Contents

List of Contributors

Haleh Ahmadian
Protein Purification Technology, Novo Nordisk A/S, Måløv, Denmark

Satinder Ahuja
Ahuja Consulting, Calabash, NC, USA

Niklas Andersson
Chemical Engineering, Lund University, Lund, Sweden

Chris Antoniou
Biogen, Cambridge, MA, USA

Suvrajit Banerjee
Department of Chemical and Biological Engineering, Rensselaer Polytechnic Institute, Troy, NY, USA

Marc Bisschops
Pall Corporation, Medemblik, the Netherlands

Martin P. Breil
DAPI Modelling & Optimization, Novo Nordisk A/S, Bagsværd, Denmark

Nina Brestrich
Institute of Engineering in Life Sciences, Section IV: Biomolecular Separation Engineering, Karlsruhe Institute for Technology, Karlsruhe, Germany

Mark Brower
Merck & Co., Inc., Kenilworth, NJ, USA

Steven Cramer
Department of Chemical and Biological Engineering, Rensselaer Polytechnic Institute, Troy, NY, USA

Patrick Diederich
Peptide & Protein Purification, Novo Nordisk A/S, Bagsværd, Denmark

Søren S. Frederiksen
Mathematical Modelling, Novo Nordisk A/S, Bagsværd, Denmark

Ernst B. Hansen
Mathematical Modelling, Novo Nordisk A/S, Bagsværd, Denmark

Thomas B. Hansen
Mathematical Modelling, Novo Nordisk A/S, Bagsværd, Denmark

Sigrid Hansen
Protein Purification Development, Novo Nordisk A/S, Gentofte, Denmark

Milton T. W. Hearn
Victorian Centre for Sustainable Chemical Manufacturing, Monash University, Melbourne, Australia

Jürgen Hubbuch
Institute of Engineering in Life Sciences, Section IV: Biomolecular Separation Engineering, Karlsruhe Institute for Technology, Karlsruhe, Germany

Stephen Hunt
KBI Biopharma, Boulder, CO, USA

Francis Insaidoo
Biologics and Vaccines, Process Development and Engineering, Merck Research Labs, Kenilworth, NJ, USA

Steffen Kidal
Mathematical Modelling, Novo Nordisk A/S, Bagsværd, Denmark

Trent Larsen
KBI Biopharma, Boulder, CO, USA

Hong Li
Process Development and Engineering, Merck, Kenilworth, NJ, USA

Justin McCue
Biogen, Cambridge, MA, USA

Jørgen M. Mollerup
PrepChrom, Klampenborg, Denmark

Venkatesh Natarajan
Biogen, Cambridge, MA, USA

Bernt Nilsson
Chemical Engineering, Lund University, Lund, Sweden

Marcel Ottens
Department of Biotechnology, Delft University of Technology, Delft, the Netherlands

Silvia M. Pirrung
Department of Biotechnology, Delft University of Technology, Delft, the Netherlands

Jennifer Pollard
Process Development and Engineering, Merck, Kenilworth, NJ, USA

Tom Ransohoff
BioProcess Technology Consultants, Woburn, MA, USA

Anurag S. Rathore
Department of Chemical Engineering, Indian Institute of Technology, New Delhi, India

Frank Riske
BioProcess Technology Consultants, Woburn, MA, USA

David Roush
Biologics and Vaccines, Process Development and Engineering, Merck Research Labs, Kenilworth, NJ, USA

Lars Sejergaard
Mathematical Modelling, Novo Nordisk A/S, Bagsværd, Denmark

Sumit K. Singh
Department of Chemical Engineering, Indian Institute of Technology, New Delhi, India

Arne Staby
CMC Project Planning & Management, Novo Nordisk A/S, Bagsværd, Denmark

Jörg Thömmes
Biogen, Cambridge, MA, USA

Robert J. Todd
KBI Biopharma, Boulder, CO, USA

Nihal Tugcu
Process Development and Engineering, Merck, Kenilworth, NJ, USA

Shuichi Yamamoto
Bio-Process Engineering Laboratory, Graduate School of Medicine and School of Engineering, Biomedical Engineering Center (YUBEC), Yamaguchi University, Ube, Japan

Noriko Yoshimoto
Bio-Process Engineering Laboratory, Graduate School of Medicine and School of Engineering, Biomedical Engineering Center (YUBEC), Yamaguchi University, Ube, Japan

Qing Sarah Yuan
Biogen, Cambridge, MA, USA

Series Preface

The upcoming volumes will attest to the importance and quality of books in this series. I would like to acknowledge the fellow coeditors and authors of these books for their agreement to participate in this endeavor. Lastly, I would like to thank Ms. Anita Lekhwani, Senior Acquisitions Editor at John Wiley and Sons, Inc., for approaching me to develop such a series. Together, we are confident that these books will be useful additions to the literature that will not only serve the biotechnology community with sound scientific knowledge but also inspire as they further chart the course of this exciting field.

Anurag S. Rathore
Department of Chemical Engineering
Indian Institute of Technology
New Delhi, India

Preface

This book covers various aspects of preparative chromatography, with a unique combination of academic research and industrial applications. We expect it to appeal to those in academia and industry who are involved in process development and the production of peptides and proteins, an area where the industry is typically reluctant to publicly share their knowledge because of trade secret considerations. Most of these major developments have either not been disclosed at all or exist only as oral conference contributions. This book aims to alleviate some of these gaps as we aim to supplement the academic contributions with industrial contributions. This aspect makes the treatment quite novel and unique when compared with other texts on the topic.

The book is divided into two parts: basic modeling and reviews and industrial separations/case studies. The basic modeling section aims to describe the recent developments in chromatographic theory and general approaches to research to provide increased understanding of the fundamentals behind chromatographic separation and behavior of proteins in these environments. The aim of this section is to provide a solid background in the theory of chromatography to the readers and to better prepare them for industrial case studies. Topics covered comprise the application of various approaches of modeling including computer simulations and mechanistic modeling. Chapter 1, by the editors, is designated to the general background for use of the various modeling tools and approaches.

The first section of the book contains fundamental contributions, general overviews, and reviews. Chapter 2, by Mollerup, provides a general and thorough overview of the thermodynamic tools and isotherm description necessary to model process chromatography in a double chapter. The author proposes approaches for acquiring accurate experimental data from which the model parameters in the adsorption isotherms can be estimated, in order to facilitate the use of simulation tools to the design and optimization of a chromatographic separation process.

Simulation of the performance of chromatographic separation of proteins is a powerful tool, and Chapter 3, by Nilsson and Andersson, presents a summary of the many methodologies applied to various chromatographic techniques

including ion exchange, affinity, and multimodal chromatography. Predictions of chromatographic behavior have been presented for a set of different separation problems, illustrating that a large number of common protein separation problems can be simulated quite easily with today's technology.

Chapter 4, by Yoshimoto and Yamamoto, describes simplified methods for understanding and designing chromatography processes for proteins and other biological products, with a focus on modeling of gradient elution chromatography. Simplified models based on the mechanistic model for linear gradient elution chromatography of proteins and other large molecule biological products are presented, together with several applications of the models to process design and process understanding and for bio-recognition.

Continuous processing, including chromatography, has gained much attention the last decade, and Chapter 5, by Riske and Ransohoff, presents industrial application of such multicolumn chromatography (MCC) systems for general capture. The authors suggest that the appropriateness and use of MCC in capture steps and in other parts of the downstream process depend on a number of factors, including the molecular characteristics and stability of the target molecule, the feed titer and product amount required, and the facility design and intention (multipurpose or dedicated). As industry gains more experience with MCC and other forms of continuous processing, the authors foresee that MCC is likely to be more commonly used throughout industry.

Molecular dynamics (MD) is another area that is getting much attention in recent years, and this approach will undoubtedly be key to better understanding of interactions on the molecular level and will ultimately result in better mechanistic models. This topic is described with case studies in Chapter 6, by Insaidoo, Banerjee, Roush, and Cramer. The authors summarize the current state of computational biophysics for determination of individual contributions of key interactions at an atomistic level. They conclude that there remains a significant gap in the linkage of experimental techniques (typically macroscopic) to biophysical modeling and that it is essential that these gaps be closed in order to realize the potential for rational process design.

Chapter 7, by Hansen, teaches the upscaling technique based on volumetric flow rate, which is founded in well-known chromatographic theory and equations, and the approach provides high process design flexibility. The chapter presents an overview of the underlying theory and also provides several examples of successful scale-ups on ion exchange and reversed-phase chromatography. A couple of industrial case studies related to these scale-ups are also presented. Finally, a step-by-step guide for scale-up is presented together with recommendations and a discussion of the challenges that a practitioner is likely to face.

The industrial separations section presents new and existing chromatographic unit operations and discusses how mechanistic and empirical modeling approaches are used to optimize equipment and methodologies. Equipment includes column

hardware, scale-down equipment, continuous operation mode, etc., as well as tools for monitoring and control; for example, on-, in-, and at-line equipment for improved process development and manufacturing methods. Improved methodologies comprise scaling approaches, the use of models for validation, uncertainty and robustness evaluations, and process design. A mix of industrial, equipment vendor, and academic authors contributed to this section. Chapter 8, by Antoniou, McCue, Natarajan, Thömmes, and Yuan, provides a number of examples where modeling may help in scale-up of chromatography in industry and how computational fluid dynamics (CFD) has been applied. The authors explore why column packing is such an important criterion that has to be consistent across scales, and they discuss how models can be utilized to predict column packing across scales and to perform packing consistently in an industrial environment.

Chapters 9, 10, and 11 (by Pirrung and Ottens; Diederich and Hubbuch; and Li, Pollard, and Tugcu, respectively) present industrial applications of process development, optimization, and small-scale practice. Chapter 9, among others, demonstrates the use of the high-throughput process development (HTPD) setup to generate mechanistic model parameters for process development, optimization, and design. The authors have discussed the pros and cons of the various experimental approaches, including the one-factor-at-a-time (OFAT), design of experiments (DOE), mechanistic modeling, and hybrid approaches. Chapter 10 provides guidance to process development using robot systems, including modeling/simulation of peak shapes for mechanistic modeling and validation. Factors that have been examined include the influence of pipetting precision, absorption measurements in microtiter plates, peak fractionation, flow patterns, and salt step heights in gradient elution experiments. Separate and combined effects have been qualitatively and quantitatively investigated using both experiments and simulations based on a mechanistic model. The authors demonstrate that with a sufficient number of fractions collected per peak, a significant improvement in precision can be obtained despite low analytical precision. Finally, Chapter 11, focuses on DOE and OFAT in an HTPD setup and presents the state-of-the-art experimental process development approach. A methodology for lab-scale chromatography process development utilizing high-throughput tools in conjunction with traditional column-based methodologies has been presented. The proposed experimental plan for process development relies heavily on a DOE approach supplemented with OFAT experiments. It fully utilizes HTPD and transitions into lab-scale column experiments where additional confirmation is required for defining parameter ranges and scale-up.

Chapters 12, 13, and 14 (by Breil, Frederiksen, Kidal, and Hansen; Hunt, Larsen, and Todd; and Sejergaard, Ahmadian, T.B. Hansen, Staby, and E.B. Hansen, respectively,) present three industrial case studies of mechanistic modeling for use in-process development, optimization, challenge, and

identification of critical process parameters, troubleshooting, deviation handling, control strategy setup, and establishing a design space for chromatographic purification. Also included are equation systems and computer coding that may help new applicants in setting up models. Chapter 13 presents an example where the general rate model has been used to describe transport behavior in the column and in the beads and the steric mass action binding model to describe protein binding to the resin matrix. This approach has been used successfully to describe the primary mechanisms involved in cation exchange chromatography of proteins. An open-source chromatography solver was used to estimate model parameters and evaluate the impact of operating parameters on process performance. Model parameters were estimated by performing a set of specific model calibration experiments. Pulse injection experiments were used to estimate the general rate model transport parameters, while steric mass action binding parameters were estimated by backfitting the model to a set of fractionated gradient elution runs. Chapter 14 discusses a specific application involving the use of a size-exclusion chromatography step for reducing aggregated product forms for the commercial production of turoctocog alfa. It has been illustrated how the different quality by design (QbD) elements of risk assessment and process knowledge can be linked through identification of key critical quality attributes (CQAs), which may be affected by the step and the different process parameters responsible for such influence on the CQAs.

Continuous processing including chromatography has gained much attention in the last decade, and Chapter 15, by Bisschops and Brower, presents industrial applications of such MCC systems for dynamic simulations as predictive models for MMC separation. This chapter describes a numerical simulation approach for predicting the performance of continuous chromatographic separations of biopharmaceutical proteins. The numerical simulations are based on the linear driving force model for mass transfer kinetics and a Langmuir isotherm for equilibrium behavior. The numerical simulations have been compared with the experimental capture efficiency of monoclonal antibodies on Protein A media in a continuous MCC system for two different monoclonal antibodies and two different (agarose based) Protein A media. The authors demonstrate the possibility of using simulation models for process characterization, thereby enabling the knowledge space with limited experimentation significantly speeding up the development program.

Chapter 16, by Rathore and Singh, presents the general state of the art of multivariate data analysis and review of current process analytical technology (PAT) methods available to facilitate process chromatography. This chapter presents a review of chemometrics applications in process chromatography. The various data preprocessing methods and modeling approaches have been discussed along with two case studies illustrating the utility of chemometrics in analyzing process chromatographic data.

Process control and PAT are topics of great interest in the industry, and new tools that may move the analytical release test burden to the unit operation process control are highly desirable. A recent tool exploiting UV spectra for this application is shown in Chapter 17, by Hansen, Brestrich, Staby, and Hubbuch. The proposed tool has a response time of <1 s and allows real-time pooling decisions. Both the screening and the PAT tool have been based on partial least squares (PLS) regression models, correlating mid-UV protein absorption spectra with selective protein concentrations. The fundamentals of intrinsic protein absorption and PLS as well as their application for selective protein quantification have been also addressed.

Finally, Chapter 18, by Hearn, presents the more sustainable and green approach to chromatographic separation and to many practical considerations needed in future manufacturing. This chapter examines recent progress toward the incorporation of the concepts underlying sustainable manufacturing of protein-based products, with emphasis of the downstream aspects of the recovery and purification of value-added protein products derived from biotechnological procedures. Lessons gained from the use of similar approaches developed within the chemical, traditional pharmaceutical, and food ingredient industries have been examined in terms of their applicability to the downstream processing of protein products derived from genetic engineering, cell culture, and associated biotechnology strategies.

The book may be read for individual contributions; however, all of the book chapters complement each other with state-of-the-art implementation of modeling in the biopharmaceutical industry and academic research within the field. All chapters of the book have been peer reviewed. We would like to thank all authors for their valuable contributions and hope the academic, industrial, and regulatory scientists will benefit from this book.

Arne Staby
20 December 2016 *Anurag S. Rathore*
Satinder Ahuja

1

Model-Based Preparative Chromatography Process Development in the QbD Paradigm

Arne Staby[1], Satinder Ahuja[2], and Anurag S. Rathore[3]

[1] *CMC Project Planning & Management, Novo Nordisk A/S, Bagsværd, Denmark*
[2] *Ahuja Consulting, Calabash, NC, USA*
[3] *Department of Chemical Engineering, Indian Institute of Technology, New Delhi, India*

1.1 Motivation

Preparative chromatography for separation of proteins and peptides continues to be the primary workhorse in purification of biopharmaceuticals. Numerous papers and books exist describing theory and implementation of preparative chromatography; however, this is the first book that combines academic progress in modeling with industrial implementation. Although theory and models have been available for many years, industrial usage of these tools has been scarce due to labor- and material-intensive requirements. However, with the biotech industry moving to implement the expectations underlined in the recent regulatory initiative of quality by design (QbD), interesting and outspread applications of modeling tools for commercial process development and manufacture have emerged.

1.2 Regulatory Context of Preparative Chromatography and Process Understanding

QbD expectations to biopharmaceutical production including preparative chromatography are described in the ICH quality guidelines Q8, Q9, Q10, and Q11 [1–4]. Further, ICH Q8-R2 [1] provides the overall definition of QbD in a regulatory context.

Preparative Chromatography for Separation of Proteins, First Edition.
Edited by Arne Staby, Anurag S. Rathore, and Satinder Ahuja.

> A systematic approach to development that begins with predefined objectives and emphasizes product and process understanding and process control based on sound science and quality risk management.

The focus of this book is on the underlined parts of this definition, and the framework of QbD may be outlined as presented in Figure 1.1. In the top part of the figure, the primary focus of biopharmaceuticals is the patient, and the patient needs are defined through the quality target product profile (QTPP), which in turn is affected by chemistry, manufacturing, and controls (CMC) activities. Fulfilling patients' needs places some requirements on the product, and these elements are obtained through linkage of the QTPP to the list of critical quality attributes (CQAs). The CQAs will have acceptable ranges for the manufacturer to comply with, and to obtain product of the desired quality, the process needs to be run within acceptable ranges of process parameters. Proper knowledge of how process parameters affect the product quality may be obtained through process models that may end up in a regulatory, enhanced application for approval of a design space. To control process parameters within defined ranges, process models and/or even a design space will provide some requirements to the GMP facility and linkage to the control strategy, which will include various process monitors, process analytical technology (PAT) tools, process validation, and release tests and specifications. All elements are linked through risk assessment exercises to address the risk-based approach of QbD in a regulatory setting.

Figure 1.1 (bottom) displays an example of QbD elements contained in the QbD framework for a preparative chromatography step. A key patient need is of course to get efficient treatment, and one element affecting this is to get a proper dose of the biopharmaceutical. To obtain proper dosing, the purity and among others the bioactivity of the biopharmaceutical needs to be correct. Purity is significantly affected by the peak collection criteria used in preparative chromatography, and a well-known methodology for peak collection is by UV monitoring as part of the control strategy (e.g., see Chapters 12 and 17). A proper understanding and control of the preparative chromatography process may be obtained by a mechanistic or statistical model and their boundary conditions that may define an operational design space. Thus, the idea of this linkage exercise is to obtain a complete overview of the process in a way that will elucidate, for example, how a defect in or removal of a UV monitor in a preparative chromatographic purification step will affect the patient through cascading back in the figure through a series of risk assessments. The focus of this book is to obtain "process understanding and process control based on sound science" as described earlier, and it can be visualized by observing the elements within the red circle in Figure 1.1 (top).

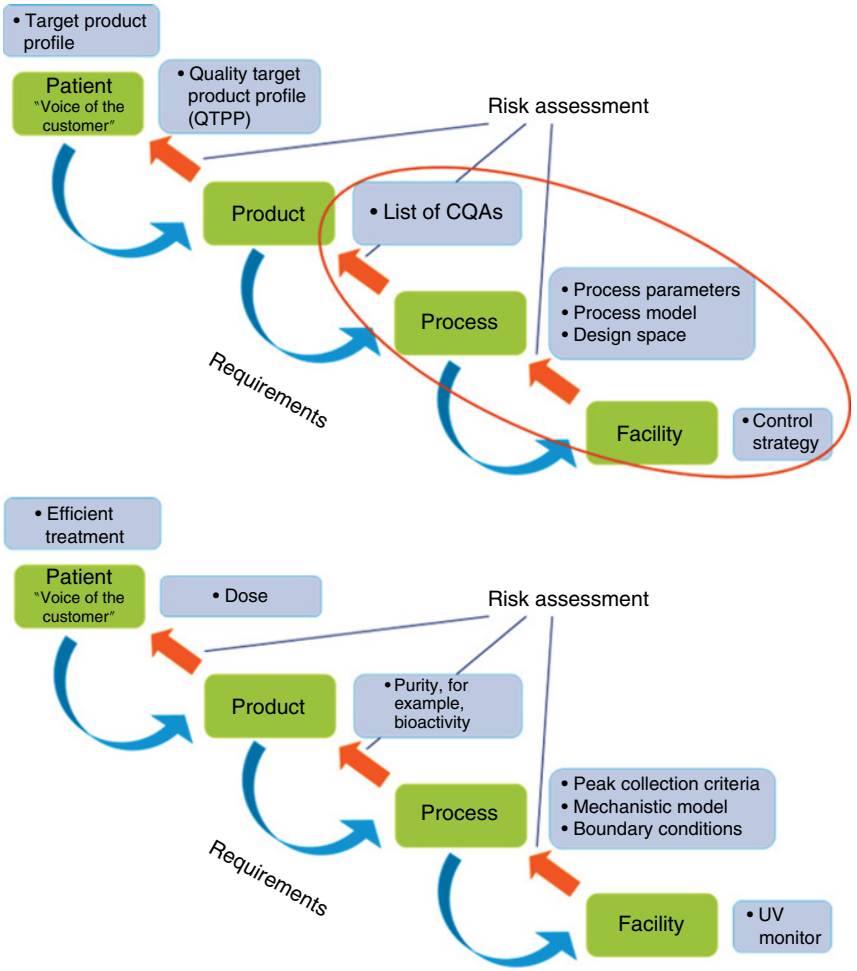

Figure 1.1 (Top) The framework of QbD. (Bottom) Example of QbD elements contained in the QbD framework for a preparative chromatography step. (*See insert for color representation of the figure.*)

A proper control strategy is achieved through sufficient process understanding. Traditionally, process understanding in the biopharmaceutical industry was obtained through a combination of theoretical knowledge based on the following: (i) education; (ii) experience from other projects and proteins optionally of similar nature, for example, mAbs; (iii) preliminary experimentation of less systematic nature; and (iv) "one parameter at a time" (OPAT) experimentation

where all variables are kept constant while systematically altering one variable. This concept has worked well for many years, and most legacy products have been developed using this approach. Figure 1.2 presents the general level of knowledge obtained by the different methodologies including more recent concepts. Although some companies have also used multivariate methods for development and documentation of legacy products, the extensive use of more advanced methods for process understanding has been affected by implementation of QbD concepts. The general methodology used in the industry today is based on multivariate statistical analysis such as design of experiments (DoE) often combined with various high-throughput process development (HTPD) techniques (see e.g., Chapter 11). DoE is a very broad and important tool that does not require mechanistic understanding prior to implementation, and it works quite efficiently if the user has prior knowledge of which parameters are significant and if the number of parameters is limited. Today, the most comprehensive application of statistical methods to support QbD and a true enhanced approach filing has been accomplished by Genentech/Roche with its recent regulatory approval of Gazyva. Disadvantages of DoE include less optimal identification of assumptions and the general lack of opportunities for extrapolation outside the experimental area used to set up the statistical models. DoE is used extensively for validation of parameter ranges in preparative chromatography; however for other unit operations

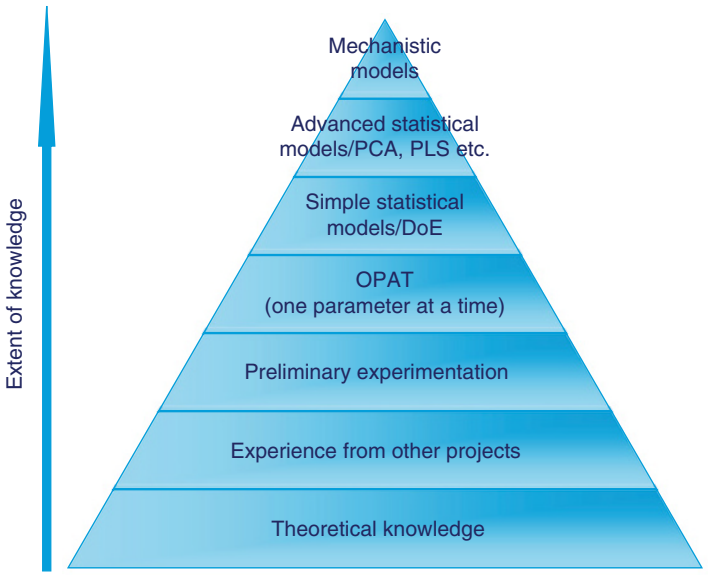

Figure 1.2 General extent of knowledge and process understanding obtained employing various methodologies and approaches.

such as fermentation, more advanced statistical methods like principal component analysis (PCA), partial least squares (PLS) methods, etc. are used due to their capability to handle very high number of variables (see also Chapter 16). At the top of the pyramid in Figure 1.2 and at the highest extent of knowledge obtainable are models based on mechanistic principles because full mechanistic process understanding is typically achieved. Depending on assumptions, these mechanistic models are also referred to as first-principle models, and they provide optimal evaluation of assumptions as well as opportunities for extrapolation outside the experimental area of parameter estimation.

An example of the difference in process understanding achieved from application of mechanistic modeling and a DoE approach for a preparative SEC step is presented in Figure 1.3 [5] (see also Chapter 14). The figure shows the effect of the feed concentration of a biopharmaceutical on the content of high molecular weight proteins (HMWP)—a typical CQA in the drug substance addressed by purification. The different experimental values for a given feed concentration (red diamonds) are due to controlled variation of other variables. Predictions based on a mechanistic model and on a statistical model by DoE are shown with full green and light blue colors, respectively. It is noticed that the model based on DoE cannot predict the worst-case conditions at a feed concentration of 0.75 g/L (indicated by the green, dashed circle) and instead the DoE-based model predicts the lowest concentration of 0.5 g/L as the worst-case conditions (indicated by the light blue, dashed circle). Further, the prediction error increases if extrapolation is performed outside the experimental area. The problem is partly caused by the general setup of

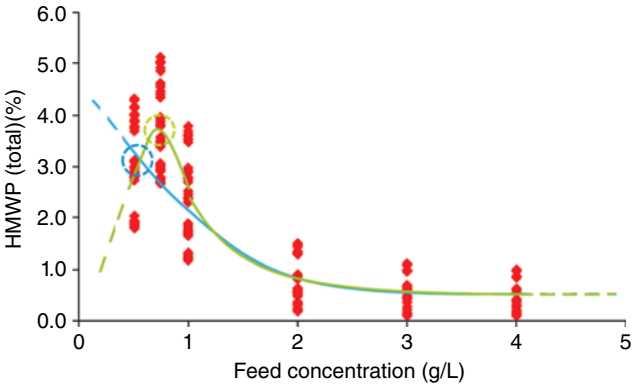

Figure 1.3 HMWP content after purification on SEC for a biopharmaceutical as a function of feed concentration. ◊, experimental results; —, model prediction by mechanistic model; and —, model prediction by statistical model based on DoE. (*See insert for color representation of the figure.*)

experiments supporting DoE where center points and parameter range limits are often applied (in the current case ~2 g/L and 0.5 and 4 g/L, respectively). DoE-based models are good in capturing monotonous functions, but they have problems capturing functions containing inflection points, and it would require a very comprehensive experimental setup for DoE-based models to capture functions with inflection points—far more than what is used in general in the industry. The experimental setup to obtain mechanistic models is typically not more comprehensive, but it is different. This example illustrates some of the pitfalls of applying DoE the way it is usually performed in the biopharmaceutical industry and how a mechanistic model may provide more process understanding.

1.3 Application of Mathematical Modeling to Preparative Chromatography

Mathematical models and modeling tools have been available for decades in academia, for example, Van Deemter [6], Giddings [7], Guiochon et al. [8], Melander and Horváth [9], Brooks and Cramer [10], Yamamoto et al. [11], Hearn et al. [12], Lenhoff [13], Carta and Jungbauer [14], Frech et al. [15], Łącki et al. [16], Hansen and Mollerup [17], Ottens et al. [18], Bracewell et al. [19] and many, many more, and the tools have been applied to academic problems such as separation of standard proteins like BSA, lysozyme, etc. and occasionally to more industry-relevant proteins. The experimental burden required and essential access to large amounts of pure experimental material made it very difficult and in fact too cumbersome for the biopharmaceutical industry to implement the methodology for many years. Motivation and requirements have, however, changed over the last years. The regulatory environment as described earlier [1–4] access to HTPD techniques [20, 21] facilitating fast experimentation and low demands of experimental material, and, in the specific case of polishing chromatography, proper assumptions and approaches to minimize the experimental task of generating preparative modeling parameters [22]. These aspects have aided the industry into initiating application of mechanistic modeling, and this book also presents numerous examples of such implementation for preparative chromatography.

Another aspect challenging the biopharmaceutical industry in implementation of mechanistic modeling tools is access to skilled personnel that can master modeling and computer coding at an expert level as well as to have comprehensive insight into preparative chromatography at manufacturing scales. Many implementation attempts in industry have failed due to lack of management support and critical mass of skilled personnel. In contrast, statistical modeling based on DoE or similar methods are much more easily implemented. An approach to initiation of implementation of mechanistic modeling is collaboration between

academics or specialized consultants and the biopharmaceutical industry, and numerous examples of such collaboration exist, for example, Borg et al. [23], Ghosh et al. [24], Rathore et al. [25], Nfor et al. [26], and many more. Another approach may be to look at trends in the small molecule pharmaceutical area, which are typically several years ahead of the biopharmaceutical industry in implementation of new tools and approaches.

New trends and hot topics in the industry include the utilization of semi- and continuous techniques (see also Chapters 5 and 15), PAT method implementation (see also Chapter 17), production of antibody–drug conjugates (ADCs) and other conjugates, and manufacturing of biosimilars, and many of these applications will benefit from the use of mechanistic modeling. As examples, the insulin purification method using MCSGP presented in Figure 1.4 was modified extensively from the original batch process by a mathematical model (L. Aumann et al., Chromacon AG, internal report to Novo Nordisk), and conjugate products that require reactions may benefit from reaction models as presented elsewhere [27]. Finally, the manufacture of biosimilars could significantly benefit from access to mechanistic modeling of preparative chromatography and other unit operations to demonstrate optimal process understanding, identification of critical process parameters, PAT-based process control, and demonstration of consistently achieving product profile that is similar to that of originator products.

Once a mechanistic model for a preparative chromatography step has been developed, the applications of the model are numerous depending on the approach and assumptions made. Figure 1.5 lists some common applications of mechanistic and statistical modeling in industry. Topics presented in black text in the figure represent themes that are covered by the subsequent book chapters, and a more thorough guidance to the individual chapters is given in the preface.

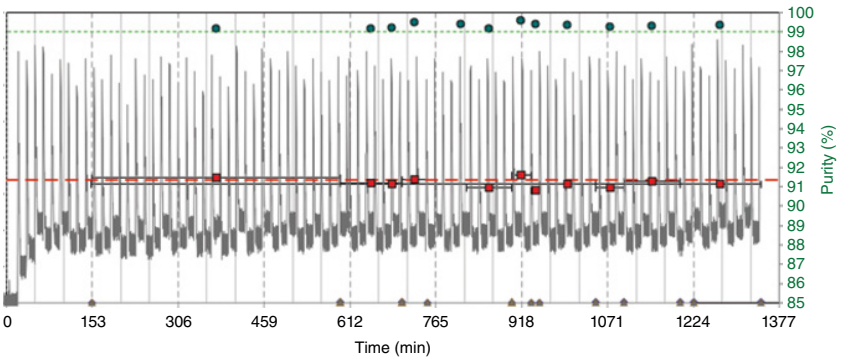

Figure 1.4 Chromatogram and purity of a three-column MCSGP unit as a function of time for a 23 h semi-continuous chromatographic purification of insulin (L. Aumann et al., Chromacon AG, internal report to Novo Nordisk).

- Process and analytical development
- Process optimization
- Process validation/challenge and critical parameters
- Plant design
- Process control (PAT)
- Troubleshooting and deviation handling
- Process understanding and design space
- Scaling of chromatography

Figure 1.5 Application options of mechanistic modeling.

Acknowledgements

The editors would like to thank all contributors of this book, as well as Thorbjørn Strøm-Hansen, Michael Schousboe, Lars Sejergaard, Marcus Degerman and Erik Skibsted, Novo Nordisk, and Lars Aumann, ChromaCon, for help with the figures of this chapter.

References

1. ICH Q8(R2) Pharmaceutical Development (2009), International Conference of Harmonization.
2. ICH Q9 Quality Risk Management (2005), International Conference of Harmonization.
3. ICH Q10 Pharmaceutical Quality System (2008), International Conference of Harmonization.
4. ICH Q11 Development and Manufacturing of Drug Substances (Chemical Entities and Biotechnological/Biological Entities) (2012), International Conference of Harmonization.
5. M. Degerman, E. Hansen, L. Sejergaard, T.B. Hansen, J. Krarup, S. Frederiksen, S. Kidal, A. Staby. Model based process development in biopharmaceutical industry—case studies. Oral keynote presentation at BPP2011, Puerto Vallarta, Mexico, September 18–22, 2011.
6. J.J. van Deemter, F.J. Zuiderweg, A. Klinkenberg. Longitudinal diffusion and resistance to mass transfer as causes of nonideality in chromatography. *Chemical Engineering Science* 5, 271–285 (1956).
7. J.C. Giddings. *Unified Separation Science*, John Wiley & Sons, Inc, New York (1991).
8. G. Guiochon, A. Felinger, D.G. Shirazi, A.M. Katti. *Fundamentals of Preparative and Nonlinear Chromatography*, 2nd edition, Academic Press, Amsterdam (2006).

9. W. Melander, C. Horváth. Salt effects on hydrophobic interactions in precipitation and chromatography of proteins: an interpretation of the lyotropic series. *Archives of Biochemistry and Biophysics* 183, 200–215 (1977).
10. C.A. Brooks, S.M. Cramer. Steric mass-action ion exchange: displacement profiles and induced salt gradients. *AIChE Journal* 38, 1969–1978 (1992).
11. S. Yamamoto, K. Nakanishi, R. Matsuno. *Ion-Exchange Chromatography of Proteins*, Marcel Dekker, New York (1988).
12. F. Lin, W. Chen, M.T.W. Hearn. Thermodynamic analysis of the interaction between proteins and solid surfaces: application to liquid chromatography. *Journal of Molecular Recognition* 15, 55–93 (2002).
13. A.M. Lenhoff. Significance and estimation of chromatographic parameters. *Journal of Chromatography A* 384, 2, 285–299 (1987).
14. G. Carta, A. Jungbauer. *Protein Chromatography: Process Development and Scale-up*, Wiley VCH Verlag GmbH & Co., Weinheim (2010).
15. M. Schmidt, M. Hafner, C. Frech. Modeling of salt and pH gradient elution in ion-exchange chromatography. *Journal of Separation Science* 37, 1–2, 5–13 (2014).
16. X. Zhang, B.A. Grimes, J.-C. Wang, K.M. Łącki, A.I. Liapis. Analysis and parametric sensitivity of the behavior of overshoots in the concentration of a charged adsorbate in the adsorbed phase of charged adsorbent particles: practical implications for separations of charged solutes. *Journal of Colloid and Interface Science* 273, 1, 22–38 (2003).
17. E. Hansen, J. Mollerup. The influence of retention on the plate height in ion exchange chromatography. *Separation Science and Technology* 39, 2011–2030 (2004).
18. B.K. Nfor, D.S. Zuluaga, P.J.T. Verheijen, P.D.E.M. Verhaert, L.A.M. van der Wielen, M. Ottens. Model-based rational strategy for chromatographic resin selection. *Biotechnology Progress* 27, 6, 1629–1643 (2011).
19. S. Gerontas, M.S. Shapiro, D.G. Bracewell. Chromatography modelling to describe protein adsorption at bead level. *Journal of Chromatography A* 1284, 44–52 (2013).
20. J.L. Coffman, J.F. Kramarczyk, B.D. Kelley. High-throughput screening of chromatographic separations: 1. Method development and column modeling. *Biotechnology and Bioengineering* 100, 605–618 (2008).
21. M. Bensch, P. Schulze Wierling, E. von Lieres, J. Hubbuch. High throughput screening of chromatographic phases for rapid process development. *Chemical Engineering & Technology* 28, 11, 1274–1284 (2005).
22. S. Kidal, T.B. Hansen, A. Staby. Methods of optimizing chromatographic separation of polypeptides. WO/2008/028974 (2008).
23. N. Borg, Y. Brodsky, J. Moscariello, S. Vunnum, G. Vedantham, K. Westerberg, B. Nilsson. Modeling and robust pooling design of a preparative cation-exchange chromatography step for purification of monoclonal antibody monomer from aggregates. *Journal of Chromatography A* 1359, 170–181 (2014).

24. P. Ghosh, K. Vahedipour, M. Lin, J.H. Vogel, C. Haynes, E. von Lieres. Computational fluid dynamic simulation of axial and radial flow membrane chromatography: mechanisms of non-ideality and validation of the zonal rate model. *Journal of Chromatography A* 1305, 30, 114–122 (2013).

25. A.S. Rathore, O. Kaltenbrunner, P. Engel, J.M. Mollerup, J. McCue. Modeling of biopharmaceutical processes. Part 2: process chromatography unit operation. *BioPharm International* 21, 8, 28–42 (2008).

26. B.K. Nfor, T. Ahamed, G.W.K. van Dedem, P.D.E.M. Verhaert, L.A.M. van der Wielen, M.H.M. Eppink, E.J.A.X. van de Sandt, M. Ottens. Model-based rational methodology for protein purification process synthesis. *Chemical Engineering Science* 89, 185–195 (2013).

27. L. Sejergaard, M.H. Hansen, A.A. Olsen, P. Østergaard, T. Strøm-Hansen, P. Østfeldt, S. Valentin, A. Staby. Implementation of unit operation design spaces: experiences with regulatory authorities. Oral presentation at 245th ACS National Meeting, New Orleans, LA, April 7–11, 2013.

2

Adsorption Isotherms

Fundamentals and Modeling Aspects

Jørgen M. Mollerup

PrepChrom, Klampenborg, Denmark

2.1 Introduction

The use of process simulation in computational fluid dynamics and in computer-aided design enables the chemical engineer to analyze, design, and optimize chemical processes. Chemical engineers use process simulators to scale up processes from bench scale to production scale in a single step. A prerequisite for doing this is the availability of models of the unit operations involved as well as models of the physical–chemical properties of the various fluids and solutions. The fulcrum point to the design of separation processes like distillation, extraction, absorption, and adsorption is the phase equilibrium properties.

To the design of a large distillation column, a chemical engineer will not use a small distillation column to investigate how to purify a product by trial and error. The engineer will use dedicated equipment to measure the vapor–liquid equilibrium data needed to determine the parameters in the phase equilibrium model and use a process simulator to design and optimize the distillation column.

The agenda in process chromatography is very similar. There is no need to collect thousands of data from a robotic system and look for some "optimal" separation conditions. The agenda is to measure some very accurate experimental data from which the model parameters in the adsorption isotherms can be estimated in order to facilitate the use of simulation tools to the design and optimization of a chromatographic separation process. The be-all and end-all are the isocratic retention volumes at analytical load from which most of the parameters in the adsorption isotherms can be estimated. These data can be performed using a rather crude feedstock and consume very little material.

Preparative Chromatography for Separation of Proteins, First Edition.
Edited by Arne Staby, Anurag S. Rathore, and Satinder Ahuja.

The parameters that determine the nonlinear behavior of the adsorption isotherm can be estimated from chromatographic runs at high load and from batch adsorption data.

2.2 Definitions

This section gives the definitions of the nomenclature used in this chapter. A schematic representation of the column is shown in Figure 2.1. There are three phases in the column. The *mobile phase* is the volume of the column where the liquid is flowing through the column. The *adsorbent* is a particle with a very high porosity and a large surface area. The ligands are not bonded directly to the surface of the solid structure of the adsorbent, but they are immobilized by means of a chain of small molecules, a spacer, in order to make it easier for the large macromolecules to associate with the ligands. Some spacers are grafted and carry several ligands. There are no ligands in the third phase, the solid support of the particle.

The *interstitial bed porosity*, ε_b, is the volume of the cavities that are between and around the adsorbents. It is difficult to measure but it is of the order of 0.37–0.45. The *particle porosity*, ε_p, is the fraction of the particle volume that is occupied by the mesopores inside the particle. The *total porosity*, ε_t, of the bed is the volume fraction of liquid phase in the bed, that is, $\varepsilon_t = \varepsilon_b + (1-\varepsilon_b)\varepsilon_p$.

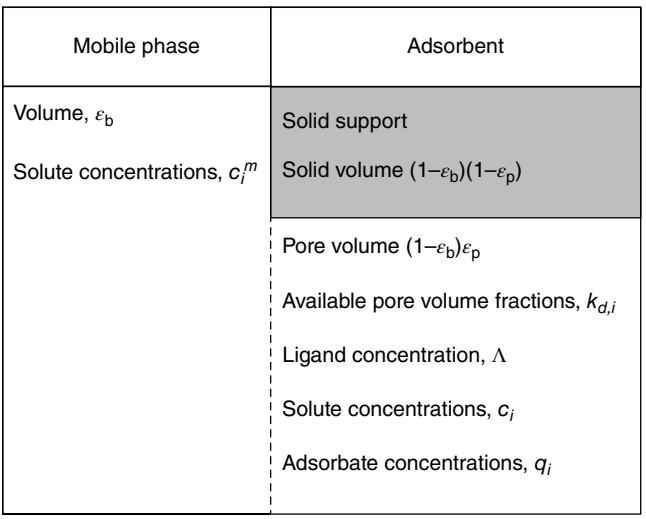

Figure 2.1 A schematic representation of a unit volume of a chromatographic column. Gray shading represents the solid-phase support which is unaffected by the interaction with mobile phase and solutes.

$k_{d,i}$ is an *exclusion factor* that represents the fraction of the stationary phase pore volume that is available for diffusion of a given solute species i; consequently $k_{d,i}$ has a value between unity and zero. By definition, $k_{d,i}$ is unity for ions of common salts like sodium chloride.

Concentrations are usually reported as molarity (moles per liter of solution), M, or millimoles per liter, mM. An *adsorbate* is a molecule that associates with a number of ligands in the adsorbent, q_i denotes the concentration of the adsorbate of species i in the pore volume, and c_i is the concentration of a solute molecule of the same species in the pore volume. q_i and c_i are equilibrium concentrations. The mobile-phase concentration of species i, c_i^{m}, is in general not in equilibrium with the corresponding pore volume concentration, c_i, due to the resistance to mass transfer. However, when isocratic retention data at analytical load are utilized to determine the parameters in the adsorption isotherm, it is assumed that the first moment of a peak represents an equilibrium property.

The *interstitial volume*, V_0, is the volume of the bed in the column, V_{c}, times the interstitial porosity, ε_{b}, that is, $V_0 = V_{\mathrm{c}}\varepsilon_{\mathrm{b}}$, and this volume is identical with the volume of the mobile phase in the column.

The *interstitial velocity*, υ, is the average linear velocity in the interstices between the particles, $\upsilon = Q/A_{\mathrm{c}}\varepsilon_{\mathrm{b}}$, where Q is the volumetric flow rate, A_{c} is the cross-sectional area of the column, and $A_{\mathrm{c}}\varepsilon_{\mathrm{b}}$ is the average cross-sectional flow area.

The holdup time or the *residence time* of the solvent, t_0, is the interstitial volume, V_0, divided by the volumetric flow rate, Q, that equals the bed height, L, divided by the interstitial velocity, that is, $t_0 = V_0/Q = L/\upsilon$.

The *phase ratio*, ϕ, is defined as

$$\phi = \frac{\text{pore volume}}{\text{interstitial volume}} = \frac{\left(1-\varepsilon_{\mathrm{b}}\right)\varepsilon_{\mathrm{p}}}{\varepsilon_{\mathrm{b}}} \tag{2.1}$$

The amount of material of species i adsorbed in a unit bed volume is $q_i\left(1-\varepsilon_{\mathrm{b}}\right)\varepsilon_{\mathrm{p}}$.

There is an extensive list of glossary of terms in Ref. [1]. In this chapter the following terms are utilized:

Convex and concave: A function is convex if the second derivative, $f''(x)$, is positive, and if the second derivative, $f''(x)$, is negative, the function is concave. The point where $f''(x)$ is zero is an inflection point. In the literature convex is also called convex downward or concave upward, and concave is also called concave downward or convex upward.

Curvature: The curvature is the second derivative of a function.

Eluate: The mobile phase at the column exit containing some feed components, the eluites.

Elution: Purification or separation of the feed components by an eluant flowing through the column.

Eluant: Synonymous with the pure mobile phase at the column inlet.
Eluite: A component in the feed, dissolved in the mobile phase, at the column exit.
Elution profile: The plot of the concentration of the eluite component versus the volume of the mobile phase passed. Usually, it is a wide, unsymmetrical peak, such as those obtained under nonlinear conditions. Guiochon et al. prefer the term band profile.
Fronting: A type of peak asymmetry in which the rear is steep and the front rises slowly from the baseline. It is often due to a convex isotherm.
Modulator: Additives, usually salts and solvents, added to the eluant to adjust the elution of components in the feed that can adsorb to the ligands.
Solute: A component in solution in a fluid phase. In this chapter, a distinction is made between solutes, salts, and solvents.
Solvent: A water-soluble liquid added to the eluant or to the feed solution.
Tailing: A type of peak asymmetry in which the front is steep and the rear returns slowly to the baseline. It is often due to a concave isotherm.

2.3 The Solute Velocity Model

The solute velocity model is fundamental to the understanding and interpretation of the elution profiles. The model will be utilized to calculate the shape of elution profiles in ideal chromatography. Ideal chromatography [1, page 958] is a model of chromatography assuming no axial dispersion and no mass transfer resistance. It permits an easy study of the influence of the thermodynamics of phase equilibrium (i.e., of the adsorption isotherm) on the elution profiles.

The average linear velocity of the mobile phase is the interstitial velocity, υ, but a molecule that adsorbs will move at a lower velocity because the adsorption–desorption process slows down the solute velocity. When a molecule of species i associates with the ligands, the overall concentration, s_i, in the pore volume increases from $s_i = c_i$ to $s_i = c_i + q_i$. Guiochon et al. [1, Section 8.1] have shown that the *solute wave velocity*, u_i, of a single solute at isocratic conditions is

$$u_i = \frac{\upsilon}{1 + \phi k_{d,i} \partial s_i / \partial c_i} = \frac{\upsilon}{1 + \phi k_{d,i} \left(1 + \partial q_i / \partial c_i\right)} \tag{2.2}$$

The solute wave velocity depends on the slope of the adsorption isotherm, $\left(\partial q_i / \partial c_i\right)$, and that explains why the shape of the elution profile depends on the slope of the adsorption isotherm.

The classical adsorption isotherm has a *negative curvature*, that is, $\left(\partial^2 q_i / \partial c_i^2\right) < 0$. An example is shown in Figure 2.3, which shows the adsorption isotherm of a GLP-1 derivative, the slope of the isotherm, and q_i/c_i. When the adsorption isotherm has a negative curvature, the slope of the adsorption

isotherm decreases with increasing solute concentration; wherefore the solute velocity will increase with increasing solute concentration as shown in Figure 2.4. Theoretically this will lead to a situation where the lower part of a leading edge of an elution profile moves at a lower velocity than the top of the leading edge. This is physically impossible. The difference in solute velocities leads to a compression of the front of the elution profile resulting in a shock wave [1, Section 14.1.4] moving at the velocity

$$u_i = \frac{\upsilon}{1+\phi k_{d,i}\Delta s_i/\Delta c_i} = \frac{\upsilon}{1+\phi k_{d,i}\left(1+\Delta q_i/\Delta c_i\right)} \tag{2.3}$$

Here $(\Delta q_i/\Delta c_i)$ is the slope of the cord of the adsorption isotherm of species i, and Δc_i is the step-up in the concentration at the leading edge. $\Delta q_i/\Delta c_i$ is not necessarily identical with q_i/c_i unless the step-up is from a concentration equal to zero. The diffuse wave velocity and the shock wave velocity of a GLP-1 derivative are shown in Figure 2.4.

In the absence of dispersion forces, the shock wave will be vertical; wherefore the shape of a leading edge is determined by the competition between the dispersion forces and the shock wave that counteracts the dispersion forces. At the rear of the elution profile, where the concentration decreases, the dispersion forces and the decreasing solute velocity will act in the same direction and create an elution profile with a positive curvature, a *diffuse wave*. A series of simulated elution profiles of a GLP-1 derivative are shown in Figure 2.5.

Some adsorption isotherms have a *positive curvature*, that is, $\left(\partial^2 q_i/\partial c_i^2\right) > 0$ at low solute concentration due to self-association of the proteins. This means that proteins act as ligands themselves. An example is shown in Figure 2.17, which shows the adsorption isotherm, the slope of the adsorption isotherm, and the ratio q_i/c_i of a GLP-1 analogue. When the adsorption isotherm has a positive curvature, the slope of the adsorption isotherm increases with increasing solute concentration; wherefore the solute velocity will decrease with increasing solute concentration. The result is that the leading edge of the elution profile will be a diffuse wave and the rear of the elution profile will be a shock wave at low solute concentration. Figure 2.19 shows the diffuse wave velocity and the shock wave velocity of a GLP-1 analogue, and a series of simulated elution profiles are shown in Figure 2.20.

The elution time of a wave is

$$\frac{t_i}{t_0} = \frac{\upsilon}{u_i} \tag{2.4}$$

If volume units are preferred, the corresponding equation is

$$\frac{V_i}{V_\mathrm{c}} = \frac{\upsilon\varepsilon_\mathrm{b}}{u_i} \tag{2.5}$$

A Dirac's delta function is a function that has unit area, the width h, and the height $1/h$ where $h \to 0$. If the adsorption isotherm is linear and a sample that resembles a Dirac's delta function is injected into the column, the resulting response at the column outlet is an elution profile that has the shape of a Gaussian distribution. A linear adsorption isotherm has a constant slope where

$$\lim_{c_i \to 0}\left(\frac{\partial q_i}{\partial c_i}\right) = \lim_{c_i \to 0}\left(\frac{q_i}{c_i}\right) \equiv A_i \tag{2.6}$$

A_i is the *thermodynamic retention factor* of species i. When the solute velocity is independent of the solute concentration, the retention time, $t_{\mathrm{R},i}$, the first moment of the Gaussian peak in time units, is calculable from Equations 2.2, 2.4, and 2.6, that is,

$$t_{\mathrm{R},i} = t_0\left(1 + \phi k_{d,i}\left(1 + A_i\right)\right) \tag{2.7}$$

If volume units are preferred, the corresponding equation is

$$V_{\mathrm{R},i} = V_{\mathrm{c}}\left(\varepsilon_{\mathrm{b}} + \left(1 - \varepsilon_{\mathrm{b}}\right)\varepsilon_{\mathrm{p}} k_{d,i}\left(1 + A_i\right)\right) \tag{2.8}$$

The second central moment, the variance, σ^2, of the Gaussian peak is determined by the dispersion forces and the retention time alone. The model of the second central moment is known as the van Deemter equation [2], and its applications are analyzed in Ref. [1, Section 6.2.2] and in [3, 4].

In size exclusion chromatography, as well as in other chromatographic techniques, the porous structure retains the species simply because the molecules can diffuse into some of the openings. When there is no adsorption–desorption taking place, the thermodynamic retention factor, A_i, in Equation 2.8 is zero, and the retention volume due to the pore diffusion is

$$V_{NA,i} = V_{\mathrm{c}}\left(\varepsilon_{\mathrm{b}} + \left(1 - \varepsilon_{\mathrm{b}}\right)\varepsilon_{\mathrm{p}} k_{d,i}\right) \tag{2.9}$$

The retention volume of a common salt, where $k_{d,i}$ by definition is unity, is

$$V_{\mathrm{salt}} = V_{\mathrm{c}}\left(\varepsilon_{\mathrm{b}} + \left(1 - \varepsilon_{\mathrm{b}}\right)\varepsilon_{\mathrm{p}}\right) = V_{\mathrm{c}}\varepsilon_{\mathrm{t}} \tag{2.10}$$

The retention factor, k_i', in gas chromatography is

$$k_i' = \frac{t_{\mathrm{R},i} - t_0}{t_0} = \frac{V_{\mathrm{R},i} - V_0}{V_0} \tag{2.11}$$

k_i' is a convenient measure of the relative retention in an open tubular column where the stationary phase is coated to the interior surface of the tube. However,

in liquid column chromatography where the stationary phase is porous beads, it is convenient to correct for the pore diffusion and use the quantity

$$R_i = \frac{V_{\mathrm{R},i} - V_{NA,i}}{V_{\mathrm{c}}} = \left(1 - \varepsilon_{\mathrm{b}}\right)\varepsilon_{\mathrm{p}} k_{d,i} A_i \tag{2.12}$$

as a measure of the *relative retention* due to the adsorption. This quantity is the retention due to the adsorption per unit column volume, and it can be calculated directly from experimental data and does not require any knowledge of the porosities.

2.4 Introduction to the Theory of Equilibrium

The reason to include this section is to analyze similarities and differences in the application of the equilibrium theory for three different systems. The first example is an analysis of the equilibrium between two fluid phases. The second example is a reversible reaction in a single-phase system, and the last example is an analysis of a reversible adsorption. The traditional-phase equilibrium system is included in the analysis to illustrate the difference between adsorption equilibria and traditional-phase equilibria.

2.4.1 Phase Equilibria

It is a consequence of the second law of thermodynamics that an isolated system will approach equilibrium by increasing its entropy and that the equilibrium state is a stationary point of maximum entropy [5].

In consequence of this, two fluid phases are in equilibrium when the temperature, T, and the pressure, p, of the two phases are identical and when an intensive variable called the chemical potential, μ_{i}, of any component, i, is identical in the two phases. If the two phases are denoted by α and β, respectively, the necessary conditions that characterize a system at equilibrium are

$$T^{(\alpha)} = T^{(\beta)} \tag{2.13}$$

$$p^{(\alpha)} = p^{(\beta)} \tag{2.14}$$

$$\mu_i^{(\alpha)} = \mu_i^{(\beta)}; \quad \text{at all species i in the system} \tag{2.15}$$

The chemical potentials are calculable as partial molar derivatives of the Gibbs energy:

$$G\left(T, p, \mathbf{n}\right) = \sum_{1}^{N} n_i \mu_i \left(T, p, \mathbf{n}\right) \Leftrightarrow \mu_i = \left(\frac{\partial G}{\partial n_i}\right)_{T,p} \tag{2.16}$$

where **n** is a composition vector, in mole numbers, of the system, $n_1, n_2, \ldots, n_i, i = 1, N$, and where N is the number of components in the system. If electrolytes are present, the specification of the charges of the ionic species and the dielectric properties of the solvent are needed to characterize the system, a subject analyzed in the Appendix.

The equilibrium conditions, Equations 2.13–2.15, are necessary but not sufficient conditions to ensure that the system is stable. The number of phases in a system at equilibrium is determined from the condition that the value of the Gibbs energy is at its global minimum. That is, the system is stable if, for any changes that can be made in the closed system [5, Chapter 8],

$$(\Delta G)_{T,p} > 0 \tag{2.17}$$

If a three-phase equilibrium system has a lower Gibbs energy than the corresponding two-phase system, the three-phase system will be the stable one. A trivial case is that a one-phase system has the lowest Gibbs energy of all.

The condition that the value of the Gibbs energy in a closed system at equilibrium is at its global minimum is a consequence of the fact that the equilibrium state is a state where the value of the entropy is at its global maximum, that is, a stationary point of maximum entropy.

2.4.2 Reversible Chemical Reaction

The second system is a single-phase system where a reversible chemical reaction takes place. The system is an isothermal and isobaric system where the components A and B react to form a new component D. The reaction scheme is

$$\mathrm{A} + \nu \mathrm{B} \rightleftharpoons \mathrm{D} \tag{2.18}$$

where ν is a stoichiometric coefficient. Equation 2.18 is the overall reaction scheme, and it does not provide any information of the reaction pathway and the kinetics.According to the condition given in Equation 2.17, the system is at equilibrium when the Gibbs energy of the system is at its global minimum; wherefore

$$\Delta G = \mu_{\mathrm{D}} - \mu_{\mathrm{A}} - \nu\mu_{\mathrm{B}} = 0 \tag{2.19}$$

that is, when any displacement in the reaction equilibrium will increase the Gibbs energy of the system.

2.4.3 Adsorption of a Single Component

Reversible adsorption equilibria are thermodynamically speaking similar to reversible reaction equilibria because the proteins associate with the immobilized ligands and this association adds a new "component" to the system.

The condition that determines the equilibrium is therefore the one given in Equation 2.19 and not the condition given in Equation 2.15.

When a protein molecule, P, associates with ν ligands, L, to form an association complex, PL_ν, the equilibrium scheme is

$$P + \nu L \rightleftharpoons PL_\nu \tag{2.20}$$

and at equilibrium, it must hold that the value the Gibbs energy is at its global minimum, that is,

$$\Delta G = \mu_{PL_\nu} - \mu_P - \nu\mu_L = 0 \tag{2.21}$$

It is convenient to analyze Equation 2.21 in detail and work out a simple model for the adsorption isotherm. In order to utilize the equilibrium conditions given in Equation 2.21 to calculate the equilibrium concentrations, a relationship between the chemical potentials and the mole fractions, x_i, must be set up. The general expression for the chemical potentials is analyzed in Section 2.A.1.2. The general expression is

$$\mu_i(T, p, \mathbf{n}) = \mu_i^0(T, p) + \mu_i^E(T, p, \mathbf{n}) + RT \ln x_i \tag{2.22}$$

where $\mu_i^0(T, p)$ are the reference state chemical potentials and $\mu_i^E(T, p, \mathbf{n})$ are the excess potentials. For simplicity, it is in this analysis assumed that the excess potentials are zero because the scope of the analysis is to illustrate the fundamental principles alone. When the chemical potential model is inserted in Equation 2.21, the result is an equation that enables calculation of the equilibrium composition:

$$\mu_{PL_\nu}^0(T, p) - \mu_P^0(T, p) - \nu\mu_L^0(T, p) + RT\left(\ln x_{PL_\nu} - \ln x_P - \nu \ln x_L\right) = 0 \tag{2.23}$$

The reference state chemical potentials define the thermodynamic equilibrium constants, K, where

$$RT \ln K = -\left(\mu_{PL_\nu}^0(T, p) - \mu_P^0(T, p) - \nu\mu_L^0(T, p)\right) \tag{2.24}$$

The equilibrium constant is a function of temperature and pressure alone. The relationship between mole fractions, x_i, and molar concentrations, c_i, is

$$x_i = \frac{c_i}{\sum_{j=1}^{N} c_j} = \frac{c_i}{c} \tag{2.25}$$

where c is the molar density of the solution. Inserting Equations 2.24 and 2.25 in Equation 2.23 gives a relation between the composition, in either mole fractions or molarities, and the thermodynamic equilibrium constant:

$$K = \frac{x_{\mathrm{PL}_\nu}}{x_{\mathrm{P}} x_{\mathrm{L}}^{\nu}} = \frac{c_{\mathrm{PL}_\nu} c^{\nu}}{c_{\mathrm{P}} c_{\mathrm{L}}^{\nu}} \tag{2.26}$$

In a chromatographic adsorbent there is a constraint on the system; the density of the immobilized ligand, Λ (mol/L of pore volume), is fixed; wherefore a material balance provides the constraint that

$$\Lambda = c_{\mathrm{L}} + \nu c_{\mathrm{PL}_\nu} \tag{2.27}$$

The theoretical maximum adsorption capacity is Λ/ν. In reality, the maximum available capacity is less, often only 40–50% or less of the theoretical capacity. When Equation 2.27 is used to eliminate the concentration of available ligands, c_{L}, the resulting equation provides a relationship between the solute concentration, c_{P}, and the concentration of the protein associated with ν ligands, c_{PL_ν}:

$$K = \frac{c_{\mathrm{PL}_\nu}}{c_{\mathrm{P}}} \left(\frac{c}{\Lambda - \nu c_{\mathrm{PL}_\nu}} \right)^{\nu} \Leftrightarrow \frac{c_{\mathrm{PL}_\nu}}{c_{\mathrm{P}}} = K \left(\frac{\Lambda}{c} \right)^{\nu} \left(1 - \frac{c_{\mathrm{PL}_\nu}}{\Lambda/\nu} \right)^{\nu} \tag{2.28}$$

Using the traditional notation, the protein concentration in the adsorbed state, the adsorbate concentration, c_{PL_ν}, is replaced by q and Λ/ν by $q^{\max}$, and the eventual result is

$$\frac{q}{c_{\mathrm{P}}} = K \left(\frac{\Lambda}{c} \right)^{\nu} \left(1 - \frac{q}{q^{\max}} \right)^{\nu} \tag{2.29}$$

If there is only one association site between the protein and the ligand, that is, $\nu = 1$, the model becomes identical with the Langmuir adsorption isotherm:

$$\frac{q}{c_{\mathrm{P}}} = K \left(\frac{\Lambda}{c} \right) \left(1 - \frac{q}{q^{\max}} \right) = A \left(1 - \frac{q}{q^{\max}} \right) \quad \Leftrightarrow \quad q = \frac{A q^{\max} c_{\mathrm{P}}}{q^{\max} + A c_{\mathrm{P}}} = \frac{b q^{\max} c_{\mathrm{P}}}{1 + b c_{\mathrm{P}}} \tag{2.30}$$

where $A = bq^{\max}$. Note that it has been assumed that the solution behaves like an ideal solution because the excess potentials have been disregarded. The model applies neither to ion exchange chromatography, where the adsorption–desorption of the counterion must be included in the equilibrium scheme, nor to hydrophobic interaction chromatographic techniques because the excess potentials are not included, but nonetheless, it has found widespread application.

If competitive adsorption takes place, the multicomponent form of Equation 2.30 is

$$q_i = \frac{A_i c_i}{1 + \sum_j A_j c_j / q_j^{\max}} \tag{2.31}$$

2.5 Association Equilibria

It is a fundamental assumption [6] that the classical adsorption equilibrium entails a reversible association of some functional groups of the proteins with the functional groups of the immobilized ligands of the stationary phase and that adsorption–desorption of proteins on ion exchange adsorbents involve desorption–adsorption of small ions [7]. The interactions may also involve reversible associations of proteins to form various kinds of oligomers, displacement of water and small ions from the surface of the proteins, and interactions of solvents and additives with the proteins as well as the ligands.

Models of adsorptions isotherms can be derived from a general association scheme and the corresponding equilibrium conditions. The general association scheme is

$$\nu_{i,1} b_{i,1} + \nu_{i,2} b_{i,2} + \cdots \rightleftharpoons \nu_{i,j} b_{i,j} + \cdots + \nu_{i,m} b_{i,m}\,; \quad i = 1, 2, \ldots, \alpha \tag{2.32}$$

where $b_{i,j}$ designates the various species, $\nu_{i,j}$ designates the corresponding stoichiometric coefficients, subscripts, $i = 1, 2, \ldots, \alpha$, indicate the various association equilibria, and subscripts, $j = 1, 2, \ldots, m$, indicate the species in adsorption equilibrium number i.

When the association reactions have reached equilibrium, it must hold that the value of the Gibbs energy is at its global minimum, that is,

$$\Delta G_i = \sum_{j=1}^{m} \nu_{i,j} \mu_{i,j}(T, p, \mathbf{n}) = 0; \quad i = 1, 2, \ldots, \alpha \tag{2.33}$$

Here G is the Gibbs energy, and $\mu_{i,j}(T, p, \mathbf{n})$ is the chemical potential of species j in association reaction number i.

A general thermodynamic expression for the chemical potentials is

$$\mu_{i,j}(T, p, \mathbf{n}) = \mu_{i,j}^0(T, p) + \mu_{i,j}^E(T, p, \mathbf{n}) + RT \ln x_{i,j} \tag{2.34}$$

where $\mu_{i,j}^0(T, p)$ are the reference state potentials, $\mu_{i,j}^E(T, p, \mathbf{n})$ are the excess potentials, and $x_{i,j}$ are the mole fractions. The excess potentials include all potentials except the reference potential, that is, when electrolytes and other

charged species are present in the solution, the electric potentials must be included in the excess potentials as analyzed in Section 2.A.1.5.

For the sake of brevity, the arguments will be omitted in the rest of this section and in all subsequent sections, but the Appendix provides the necessary details.

Combining Equations 2.33 and 2.34 shows that at equilibrium, for all $i = 1, 2, \ldots, \alpha$,

$$\sum_{j=1}^{m} \nu_{i,j} \mu_{i,j}^{0} + \sum_{j=1}^{m} \nu_{i.j} \mu_{i,j}^{E} + RT \sum_{j=1}^{m} \nu_{i,j} \ln x_{i,j} = 0 \tag{2.35}$$

It is convenient to define two auxiliary variables, namely, the equilibrium constants, K_i, and the equilibrium excess functions, Γ_i. The thermodynamic equilibrium constants, K_i, are defined as

$$RT \ln K_i \equiv -\sum_{j=1}^{m} \nu_{i,j} \mu_{i,j}^{0}; \quad i = 1,2,\ldots,\alpha \tag{2.36}$$

Similarly, the equilibrium excess functions, Γ_i, which account for all deviations from ideal solution behavior, are defined as

$$RT \ln \Gamma_i \equiv -\sum_{j=1}^{m} \nu_{i,j} \mu_{i,j}^{E}; \quad i = 1,2,\ldots,\alpha \tag{2.37}$$

The excess potentials are calculable from excess Gibbs energy models, electrostatic models, and equations of state or similar state function-based models, a subject analyzed in the Appendix.

The equilibrium relations, Equation 2.35, can be written in a neater form:

$$\ln K_i + \ln \Gamma_i = \sum_{j=1}^{m} \nu_{i,j} \ln x_{i,j}; \quad i = 1,2,\ldots,\alpha \tag{2.38}$$

or

$$K_i \Gamma_i = \prod_{j=1}^{m} x_{i,j}^{\nu_{i,j}}; \quad i = 1,2,\ldots,\alpha \tag{2.39}$$

The constraints are the material and the charge balances.

2.5.1 The Asymmetric Reference Potential

Excess potentials are zero for pure substances, but the pure state is not a convenient reference state for substances that are solids in the pure state like

salts and proteins. The problem can be circumvented by changing the reference state potentials to include the excess potentials at infinite dilution in a solvent at a predefined constant solvent composition. The excess potentials at infinite dilution must be calculated at a predefined solvent composition in order to assure that the reference state potentials can be applied for solutions in pure and in mixed solvents. Due to its ubiquity, it is convenient to use pure water, w, as the reference solvent and use the symbol $\mu_{i,j}^{E_w^\infty}$ for the excess potentials at infinite dilution in pure water. The asymmetric excess potentials are defined as

$$\tilde{\mu}_{i,j}^{E} = \mu_{i,j}^{E} - \mu_{i,j}^{E_w^\infty} \tag{2.40}$$

and the asymmetric reference potentials are defined as

$$\tilde{\mu}_{i,j}^{0} = \mu_{i,j}^{0} + \mu_{i,j}^{E_w^\infty} \tag{2.41}$$

The introduction of the asymmetric excess potentials and the asymmetric reference potentials does of course not change the values of the potentials because

$$\tilde{\mu}_{i,j}^{0} + \tilde{\mu}_{i,j}^{E} = \mu_{i,j}^{0} + \mu_{i,j}^{E} \tag{2.42}$$

However, it allows for a greater flexibility in the development of models for excess potentials including salts and proteins. The details are discussed in Sections 2.A.1.3–2.A.1.5.

When the asymmetric reference potentials are used, the thermodynamic equilibrium constants, $\tilde{K}_{i,j}$, and the equilibrium excess functions, $\tilde{\Gamma}_{i,j}$, must be defined accordingly. The definitions are

$$RT \ln \tilde{K}_i = -\left(\sum_{j=1}^{m} \nu_{i,j} \mu_{i,j}^{0} + \sum_{j=1}^{m} \nu_{i.j} \mu_{i,j}^{E_w^\infty} \right) = -\sum_{j=1}^{m} \nu_{i.j} \tilde{\mu}_{i,j}^{0} \tag{2.43}$$

$$RT \ln \tilde{\Gamma}_i = -\left(\sum_{j=1}^{m} \nu_{i.j} \mu_{i,j}^{E} - \sum_{j=1}^{m} \nu_{i,j} \mu_{i,j}^{E_w^\infty} \right) = -\sum_{j=1}^{m} \nu_{i,j} \tilde{\mu}_{i,j}^{E} \tag{2.44}$$

Note that, although $K_i \neq \tilde{K}_i$ and $\Gamma_i \neq \tilde{\Gamma}_i$, it holds that $K_i \Gamma_i = \tilde{K}_i \tilde{\Gamma}_i$; wherefore

$$\tilde{K}_i \tilde{\Gamma}_i = K_i \Gamma_i = \prod_{j=1}^{m} x_{i,j}^{\nu_{i,j}} \tag{2.45}$$

Equation 2.45 will be used in the analysis of the various adsorption models.

2.6 The Classical Adsorption Isotherm

The classical adsorption isotherm originates when proteins in solution associate with the immobilized ligands of the stationary phase. The analysis presents a common form of the adsorption isotherm that includes the ion exchange adsorption isotherm and the hydrophobic adsorption isotherm. Conformational changes of the proteins do most likely take place when the proteins bind to the ligands, but in the classical model, the proteins do not associate, that is, act as ligands themselves. This subject will be analyzed in Section 2.9.

The classical ion exchange adsorption isotherm is analyzed in Section 2.7, and the adsorption isotherm of a GLP-1 derivative including simulations and an analysis of the simulated elution profiles are presented in Sections 2.7.1–2.7.1.4. The classical hydrophobic adsorption isotherm is analyzed in Section 2.8, and two examples are given. The first example in Section 2.8.1 is an analysis of the retention of lysozyme in hydrophobic interaction chromatography (HIC), the second example in Section 2.8.2 shows an analysis of the retention of three insulin variants on similar HIC adsorbents, and in Section 2.8.3 an analysis of differences and similarities between the two examples is presented.

2.6.1 Protein Association to Immobilized Ligands

Where proteins in solution associate with the immobilized ligands of the stationary phase, the general form of the association equilibria is derived from Equation 2.32:

$$\mathrm{P}_i^{z_i} + \nu_i \mathrm{L}^{z_\mathrm{L}} \mathrm{S}_\sigma^{z_\mathrm{S}} \rightleftharpoons \mathrm{P}_i^{z_i} \mathrm{L}_{\nu_i}^{z_\mathrm{L}} \mathrm{S}_{\sigma\nu_i(1-\beta_i)}^{z_\mathrm{S}} + \nu_i \beta_i \sigma \mathrm{S}^{z_\mathrm{S}}; \quad i = 1,2,\ldots,\alpha \tag{2.46}$$

The stoichiometric coefficient, ν_i, of species i is the number of immobilized ligands, L, associated with the protein, $\mathrm{P}_i^{z_i}$, carrying the charge z_i, and $\nu_i\beta_i$ is the fraction of ligands where the counterions, S, are displaced. $\beta_i = 0$ corresponds to pure hydrophobic interactions, and $\beta_i = 1$ corresponds to ionic interactions, that is, pure ion exchange. $\sigma = z_\mathrm{L}/z_\mathrm{S}$ where z_L is the charge number of the ligand and z_S is the charge number of the counterion. If the ligands do not carry any charged groups, $\sigma = 0$.

The equilibrium relation is given in Equation 2.45, and traditionally, mole fractions are replaced by ratios of molar concentrations. The mole fractions of the adsorbates, $\mathrm{P}_i^{z_i} \mathrm{L}_{\nu_i}^{z_\mathrm{L}} \mathrm{S}_{\sigma\nu_i(1-\beta_i)}^{z_\mathrm{S}}$, are q_i/c, the mole fraction of the free counterion, $\mathrm{S}^{z_\mathrm{S}}$, is c_S/c, the mole fractions of the solute proteins, $\mathrm{P}_i^{z_i}$, are c_i/c, and the mole fraction of the ligand associated with the counterion, $\mathrm{L}^{z_\mathrm{L}} \mathrm{S}_\sigma^{z_\mathrm{S}}$, is q_L/c, where c is the overall molar concentration in the pore volume. When the mole fractions are inserted in Equation 2.45, the eventual result is

$$\tilde{K}_i \tilde{\Gamma}_i = \frac{q_i}{c} \left(\frac{c_\mathrm{S}}{c} \right)^{\nu_i \beta_i \sigma} \frac{c}{c_i} \left(\frac{c}{q_\mathrm{L}} \right)^{\nu_i} \tag{2.47}$$

If $\tilde{\mu}^0$ denotes an asymmetric reference potential in the fluid phase and $\overline{\tilde{\mu}}^{\circ}$ denotes an asymmetric reference potential in the immobilized state and these potentials are inserted in Equation 2.43, the expression for thermodynamic equilibrium constants is

$$RT\ln\tilde{K}_i = -\left(\overline{\tilde{\mu}}_i^{\circ} - \tilde{\mu}_i^0\right) - \nu_i\beta_i\sigma\left(\tilde{\mu}_S^0 - \overline{\tilde{\mu}}_S^0\right) = -\Delta\tilde{G}_i^0 + \nu_i\beta_i\sigma\Delta\tilde{G}_S^0 \tag{2.48}$$

where $\tilde{\mu}_i^0$ are the asymmetric reference potentials of the solute proteins, $\overline{\tilde{\mu}}_i^{\circ}$ are the asymmetric reference potentials of the immobilized proteins in the protein–ligand complexes, $P_i^{z_i}L_{\nu_i}^{z_L}S_{\sigma\nu_i(1-\beta_i)}^{z_S}$, $\tilde{\mu}_S^0$ is the asymmetric reference potential of the free counterion, and $\overline{\tilde{\mu}}_S^0$ is the asymmetric reference potential of the immobilized counterion. Finally, $\nu_i\beta_i\sigma$ is the number of counterions that changes state, that is, they are displaced by the proteins. The ligands do not undergo a phase change because they only exist in the immobilized state; wherefore they do not contribute. $\Delta\tilde{G}_i^0$ is the change in the reference potential of a protein when it goes from the immobilized state to the solute state, and $\Delta\tilde{G}_S^0$ is the change in the reference potential of the counterion when it goes from the immobilized state to the solute state.

The equilibrium excess functions, Γ_i, are calculable from the excess potentials. If $\tilde{\mu}^E$ denotes an asymmetric excess potential in the fluid phase and $\overline{\tilde{\mu}}^E$ denotes an asymmetric excess potential in the immobilized state, the expression for the equilibrium excess functions, defined in Equation 2.44, is

$$RT\ln\tilde{\Gamma}_i = -\left(\overline{\tilde{\mu}}_i^E - \tilde{\mu}_i^E\right) - \nu_i\beta_i\sigma\left(\tilde{\mu}_S^E - \overline{\tilde{\mu}}_S^E\right) \tag{2.49}$$

where $\tilde{\mu}_i^E$ are the asymmetric excess potentials of the solute proteins, $\overline{\tilde{\mu}}_i^E$ are the asymmetric excess potentials of the proteins in the association complexes, $P_i^{z_i}L_{\nu_i}^{z_L}S_{\sigma\nu_i(1-\beta_i)}^{z_S}$, $\tilde{\mu}_S^E$ is the asymmetric excess potential of the free counterion, and $\overline{\tilde{\mu}}_S^E$ is the asymmetric excess potential of the counterion bound to the ligand. The nature of the co-ion influences the excess properties of the proteins especially if the co-ion associates with the proteins as many divalent cations do.

The material balance including unavailable ligands, available ligands, and ligands bound to proteins is

$$\Lambda = q_L + \sum_{j=1}^{\alpha}\left(\nu_j + \lambda_j\right)q_j \tag{2.50}$$

Λ is the ligand density of the chromatographic adsorbent, and according to Brooks and Cramer [8], λ_j is the number of ligands unavailable for species j due to, for example, an unfavorable pore size distribution, shielding, or electrostatic exclusion, and q_L is the density of available ligands.

The maximum adsorption capacity is

$$q_j^{\max} = \frac{\Lambda}{\left(\lambda_j + \nu_j\right)} \tag{2.51}$$

and when Equation 2.50 is used to eliminate q_L from Equation 2.47, the model for the classical adsorption equilibria is

$$\frac{q_i}{c_i} = \tilde{K}_i \tilde{\Gamma}_i \left(\frac{c}{c_S}\right)^{\nu_i \beta_i \sigma} \left(\frac{\Lambda}{c}\right)^{\nu_i} \left(1 - \sum_{j=1}^{\alpha} \frac{q_j}{q_j^{\max}}\right)^{\nu_i} \tag{2.52}$$

The stoichiometric coefficients, especially in the ion exchange mode, depend on pH of the solution, and it is uncertain whether λ_i is independent of pH. Only experimental data can provide the correct information of the pH dependence of the maximum adsorption capacity.

2.7 The Classical Ion Exchange Adsorption Isotherm

In the classical ion exchange model, derived from Equation 2.52, β_i is unity:

$$\frac{q_i}{c_i} = \tilde{K}_i \tilde{\Gamma}_i \left(\frac{c}{c_S}\right)^{\nu_i \sigma} \left(\frac{\Lambda}{c}\right)^{\nu_i} \left(1 - \sum_{j=1}^{\alpha} \frac{q_j}{q_j^{\max}}\right)^{\nu_i} \tag{2.53}$$

The charge ratio $\sigma = z_L / z_S$ is a known quantity, usually unity. In this exposition it is assumed that the charge of the ion exchanger is impervious to pH, that is, it is a strong ion exchanger. The initial slope of the ion exchange adsorption isotherm is calculated from Equation 2.6 and is

$$A_i = \tilde{K}_i \tilde{\Gamma}_i \left(\frac{c}{c_S}\right)^{\nu_i \sigma} \left(\frac{\Lambda}{c}\right)^{\nu_i} \tag{2.54}$$

A straightforward way to calculate the thermodynamic retention factors, A_i, and the stoichiometric coefficients, ν_i, is to measure the isocratic retention volumes, $V_{R,i}$, at low to moderate salt concentrations and the isocratic retention volumes, $V_{NA,i}$, at high salt concentration and calculate the relative retentions, R_i, using Equation 2.12. The result is

$$\ln R_i = \ln\left(1 - \varepsilon_b\right)\varepsilon_P k_{d,i} + \ln \tilde{K}_i + \nu_i\left(\left(\sigma - 1\right)\ln c + \ln \Lambda\right) - \nu_i \sigma \ln c_S + \ln \tilde{\Gamma}_i \tag{2.55}$$

In order to reduce the influence of the experimental uncertainty, it is recommended that $\ln R_i \geq 0.3$.

It is convenient to depict the experimental values of $\ln R_{A,i}$ versus $\ln c_S$. If the lines are straight lines, it shows that values of $\ln \tilde{\Gamma}_i$ are independent of the salt concentration. The equilibrium excess functions, $\tilde{\Gamma}_i$, account for the excess potentials, and if they are independent of the salt concentration, it is a strong indication of that the excess potentials neutralize. If the plot is a straight-line plot, as it very often is, the slopes of the straight lines give very accurate estimates of the stoichiometric coefficients. The stoichiometric coefficients, ν_i, depend on the pH of the eluant. The equilibrium constants are calculable from the values of the intersections of the straight lines with the ordinate at $\ln c_S = 0$ and numbers of the interstitial porosity, ε_b, the porosity of the adsorbent, ε_p, and the ligand density, Λ:

$$\ln \tilde{K}_i \tilde{\Gamma}_i = \ln R_i\left(\ln c_S = 0\right) - \ln\left(1-\varepsilon_b\right)\varepsilon_P k_{d,i} - \nu_i\left(\left(\sigma - 1\right)\ln c + \ln \Lambda\right) \quad (2.56)$$

The equilibrium constant is independent of the salt concentration, and if the equilibrium excess functions do not display dependence of the salt concentration, one cannot distinguish $\tilde{K}_i$ and $\tilde{\Gamma}_i$ from one another. If a solvent, for example, ethanol or polyethylene glycol is added to the eluant, it will change the equilibrium excess functions, but it will not change the equilibrium constants if the excess potentials are normalized properly as analyzed in Section 2.5.1.

According to Equation 2.48, $\ln \tilde{K}_i$ is a linear function of the stoichiometric coefficient, which depends on pH. The change in the reference potential of a protein of species i, $\Delta\tilde{G}_i^0$, is specific to the protein–adsorbent pair. It is independent of the concentration of solvents, and it is reasonable to assume that it is independent of pH. The change in the reference potential of the salt, $\Delta\tilde{G}_S^0$, is specific to the salt–adsorbent pair, and it is independent of pH for strong electrolytes. If retention data are measured for several proteins using the same salt–adsorbent pair, $\Delta\tilde{G}_S^0$ is a common parameter.

If one saturates the column with a solution of a nitrate salt and injects a small pulse of pure water, the drop in the UV signal, when the pulse passes the detector, gives a good estimate of the retention volume of the salt. The retention volume of the salt provides the value of the total porosity, and the retention volumes of the proteins at a high salt concentration provide information of the parameters $k_{d,i}$. It is usually difficult to get information about the particle porosity; wherefore it is convenient to fix the interstitial porosity, ε_b, at a reasonable value of 0.37–0.45, and calculate ε_p and $k_{d,i}$, and check if the numbers make sense. $k_{d,i}$ is less than unity and decreases with increasing size of the molecule, and the particle porosity is usually larger than 0.5 and can be as high as 0.95 for soft gels.

The maximum adsorption capacities, q_i^{max}, can be determined from a few static capacity measurements and breakthrough experiments or by fitting the model to experimental elution profiles obtained at high column load. An example is analyzed in Section 2.7.1.4.

2.7.1 The Adsorption Isotherm of a GLP-1 Derivative

In Section 2.7.1.1 it is explained how the parameters in the adsorption isotherm were estimated from measurements of the isocratic retention volumes supplemented with measurements of the adsorption capacity. The parameters are utilized to calculate the adsorption isotherm, the diffuse wave velocity, and the shock wave velocity of a GLP-1 derivative.

In Section 2.7.1.2, the isocratic elution profiles are simulated at loads from 0.1 mM·CV (column volume) up to 8.8 mM·CV.

In Section 2.7.1.3 it is analyzed how the interplay between the diffuse wave velocity and the shock wave velocity shapes the elution profile, and the result is utilized to analyze the simulated elution profiles.

In Section 2.7.1.4 it is shown how the slope of the trailing edge of an elution profile at a high load can be utilized to calculate approximate values of the second derivative of the classical adsorption isotherm.

2.7.1.1 The Adsorption Isotherm and the Wave Velocities

The parameters in the adsorption isotherms of a GLP-1 derivative and six contaminants were estimated from the isocratic retention measurements supplemented with some capacity measurements. The adsorbent is Source 30 Q and the modulator is sodium chloride. The interstitial porosity, $\varepsilon_b = 0.45$, the particle porosity, $\varepsilon_p = 0.57$, the ligand density, $\Lambda = 0.30$ mol Eq/L pore volume, and the reference Gibbs energy change of to counterion, Cl^-, and $\Delta G_s^0/RT = 0.320$ are from Ref. [9]. Four of the components have been used in a simulation study published in Ref. [10].

Figure 2.2 shows the measured isocratic elution data at analytical load for a GLP-1 derivative and six contaminants (T. B. Hansen and S. Kidal, Novo Nordisk A/S, private communication). It is important to observe that the injected amounts are so low that the adsorption isotherm is linear. This is tested by varying the injected amount in order to prove that the first moments of the recorded peaks are independent of the injected amount.

The adsorption capacity was measured for a GLP-1 derivative but not for the impurities. In order to calculate the maximum adsorption capacities for the impurities, it was assumed that for all components

$$q_{\max,i} = \frac{\Lambda}{\nu_i + \lambda} \tag{2.57}$$

A value of $\lambda = 4$ was estimated from the capacity data measured for a GLP-1 derivative, and this number was used for the contaminants as well. The parameters are summarized in Table 2.1. Figure 2.3 shows the calculated adsorption isotherm, the slope of the isotherm, and q/c of a GLP-1 derivative with 30 mM sodium chloride in the eluant.

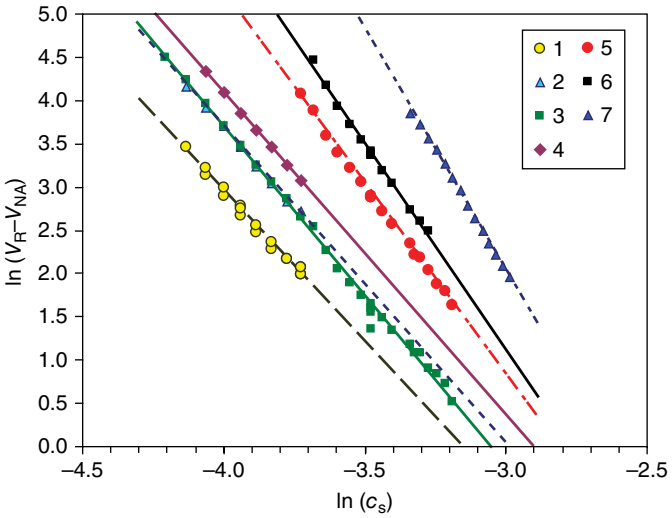

Figure 2.2 A log–log plot of the measured isocratic retention volumes of a GLP-1 derivative (■) and six contaminants on a Source 30 Q adsorbent at various sodium chloride concentrations in the eluant. (*See insert for color representation of the figure.*)

Table 2.1 Parameters for a GLP-1 derivative and six impurities estimated from the isocratic retention measurements on a Source 30 Q adsorbent.

Eluite	ν	K	$\frac{\Delta G_i^0}{RT}$	q_{max} (M)
1	3.47	0.00365	–6.72	0.0402
2	3.66	0.00459	–6.55	0.0392
3	3.90	0.00235	–7.30	0.0380
4	3.72	0.00591	–6.32	0.0389
5	4.43	0.00251	–7.40	0.0356
6	4.78	0.00185	–7.82	0.0342
7	5.53	0.00120	–8.49	0.0315

The shape of an elution profile is the result of the interplay between the diffuse wave velocity, the shock wave velocity, and the dispersion forces. Figure 2.4 depicts the calculated diffuse wave velocity and the shock wave velocity in the column with 30 mM sodium chloride in the eluant. The adsorption isotherm of the GLP-1 derivative has a negative curvature at all concentrations, and this means that the diffuse wave velocity will increase with increasing solute

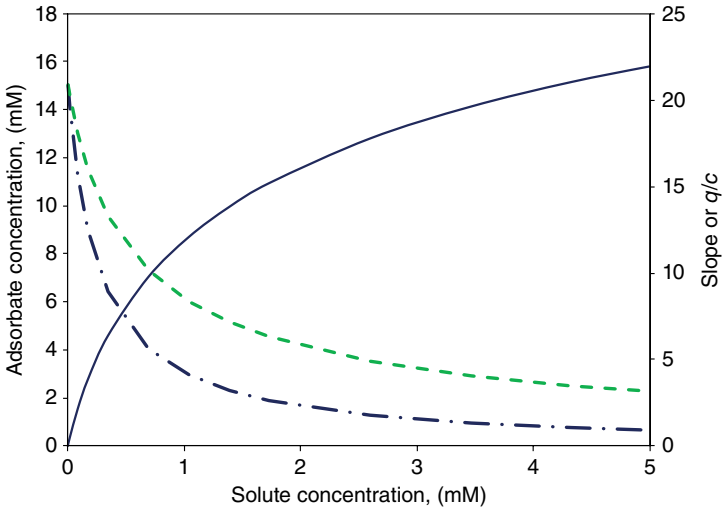

Figure 2.3 The adsorption isotherm (full line) of a GLP-1 derivative on a Source 30 Q adsorbent with 0.03 M sodium chloride in the eluant. The dashed–dotted line is the slope of the isotherm, and the dashed line is *q*/*c*.

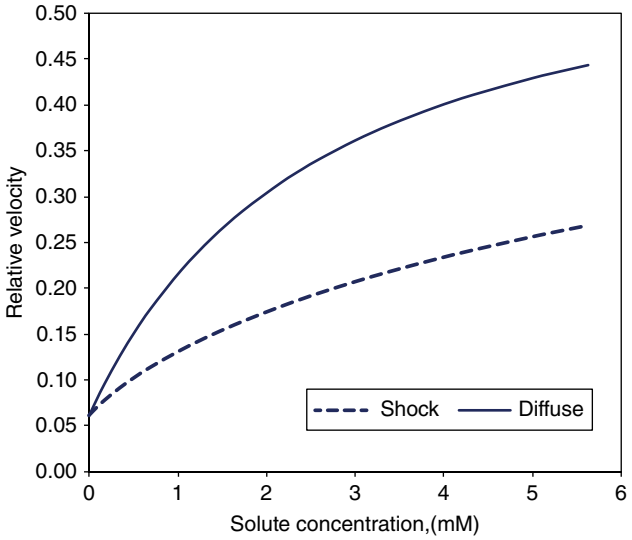

Figure 2.4 The calculated relative velocities of the diffuse wave and the shock wave of a GLP-1 derivative on a Source 30 Q adsorbent with 0.03 M sodium chloride in the eluant.

concentration. This leads to a compression at the leading edge of the elution profile; wherefore a shock wave determines the velocity at the leading edge of the elution profile. The trailing edge of the elution profile can be much curved because the diffuse wave velocity decreases with decreasing concentration and that will, in addition to the dispersion forces, increase the distance between the top and the base of the rear of the elution profile.

2.7.1.2 Simulations

Figure 2.5 depicts the result of a series of simulations. The load was varied from 0.1 to 8.8 mM·CV. The column was equilibrated with a 5 mM sodium chloride solution, and the load was a solution of 0.2 mM of a GLP-1 derivative in a 5 mM sodium chloride solution. The eluant was a 30 mM sodium chloride solution. The simulated elution profiles display the curved trailing edge that is a characteristic of the classical adsorption isotherm. The plateau at high load indicates that the elution profile reached a steady state at the leading edge. The maximum load was 8.8 mM·CV. When the load was increased to 9 mM·CV, there was a breakthrough during the load step, and part of the feed was lost. Except in a region close to the maximum of an elution profile, where the curvature is changing, the trailing edges of the simulated elution profiles are alike. In the absence of dispersion forces, all elution profiles will end at a retention volume of 7.34 CV.

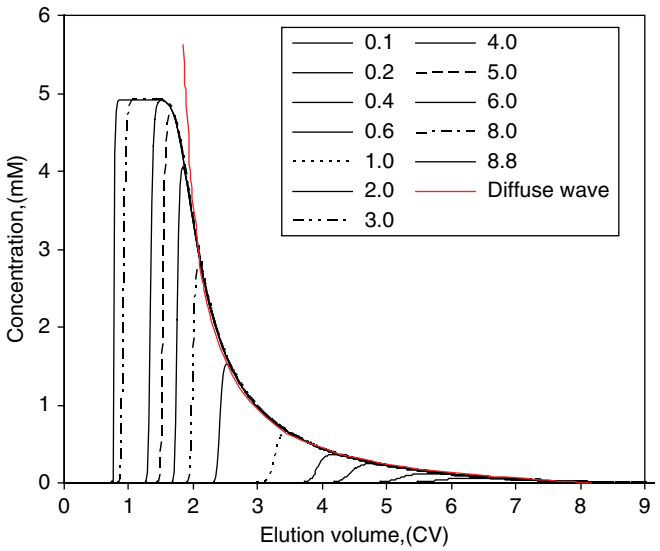

Figure 2.5 Simulated isocratic elution profiles of a GLP-1 derivative on a Source 30 Q adsorbent with 0.03 M sodium chloride in the eluant. The numbers in the legend indicate the load in mM·CV. The concentration of GLP-1 in the feed was 0.2 mM. The solid line that extends above the top of the simulated elution profiles shows the shape of the trailing edge of the ideal elution profile created by the diffuse wave.

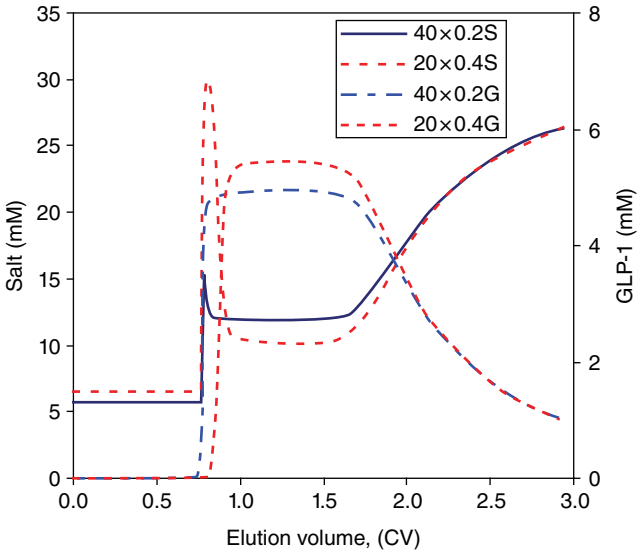

Figure 2.6 Simulated isocratic elution profiles of a GLP-1 derivative on a Source 30 Q adsorbent with 0.03 M sodium chloride in the eluant and a load of 8.8 mM·CV using two different feed concentrations. The first number in the legend is the number of column volumes loaded, and the second number is the mM concentration of GLP-1 in the feed. G means the GLP-1 elution profile, and S means the salt elution profile.

To analyze the influence of the feed concentration on the shape of the simulated elution profiles, simulations were performed where the feed volumes were decreased to one half of the values used in the first series of simulations and the concentration in the feed doubled in order to keep identical loads. At loads up to 4 mM·CV, there was no difference between the simulated elution profiles. However, when the load was increased to 5 mM·CV, a minor difference was observed, a difference that increased with increasing load. Figure 2.6 shows the elution profiles at a load of 8.8 mM·CV and the corresponding salt profiles at two different feed concentrations. The spike in the salt concentration profile started at a volume corresponding to the total porosity. The higher feed concentration gave a higher adsorbate concentration; wherefore the response from the load with the higher feed concentration gave a higher value of the concentration at the plateau. Consequently, the leading edge of this profile must elute a little later because the area under the two elution profiles must be identical as they have identical loads.

The simulations were carried out using the Craig model because it is much simpler to use especially when the adsorption equilibria become complex due to oligomer formation. In the Craig model, the dispersion due to the longitudinal dispersion and the mass transfer resistance in the system is characterized

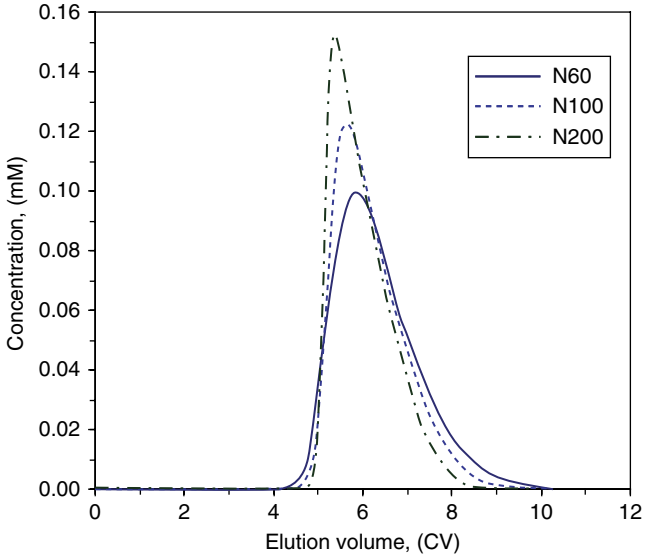

Figure 2.7 Simulated isocratic elution profiles of a GLP-1 derivative on a Source 30 Q adsorbent using 60, 100, and 200 cells in the Craig model. The eluant was a 0.03 M sodium chloride solution, and the load was 0.2 mM·CV.

by the number of cells; a high number of cells correspond to a low dispersion [1]. One hundred cells correspond to a moderate dispersion. To simulate a symmetric peak required more than a thousand cells and an extremely tiny load. The simulations shown in Figures 2.5 and 2.6 were performed using 100 cells. Figure 2.7 shows how the number of cells influenced the dispersion at a load of 0.2 mM·CV. It is easy to observe the influence of the dispersion at this low load where the adsorption isotherm is almost linear and the dispersion forces have a great influence on the second central moment of the elution profile. The influence of the number of cells on the simulated elution profiles decreases strongly with increasing load.

2.7.1.3 How the Wave Velocities Shape the Elution Profiles

The scope of this section is to analyze the simulated elution profiles shown in Figure 2.5. Chromatography is a rate-controlled separation where the shape and the position of an elution profile is the result of the interplay between the diffuse wave velocity, the shock wave velocity, and the dispersion forces. However, at preparative load, the main features of an elution profile are explained by the interplay between the two wave velocities of the solute alone. Disregarding the dispersion forces, the relation between the concentration of the eluite and the elution volume is calculable from the wave velocities using Equation 2.5 alone.

The first example is depicted in Figure 2.8. The salt concentration in the feed pulse and in the isocratic elution was 30 mM. The corresponding diffuse wave and shock wave velocities are depicted in Figure 2.4, and it is observed that the diffuse wave moves faster than the shock wave. The feed concentration was 5 mM and the feed started at $V_i = 0$ and it lasted for one column volume, that is, the load was 5 mM·CV. The feed pulse is shown as the dotted square function from 0 to 1 CV. The front of the feed pulse at $V_i = 0$ represented a step-up in the concentration from 0 to 5 mM, and this step-up created a shock wave that moved at a velocity of 0.256 times the interstitial velocity corresponding to an elution volume of 1.75 CV.

The step-down in the concentration at the end of the feed pulse at $V_i = 1$ created a diffuse wave. The diffuse wave velocity decreased with decreasing concentration, which means that the top of the trailing edge moved faster than the base of the trailing edge and that resulted in a strong tailing. At a concentration of 5 mM, the diffuse wave velocity was 0.429 times the interstitial velocity corresponding to an elution volume of 1.05 CV, and at the baseline the relative velocity was 0.061 corresponding to an elution volume of 7.34 CV.

At a concentration of 5 mM, the diffuse wave created at the rear of the feed pulse moved faster, $V_i = 1.05$, than the shock wave created at the front of the feed pulse, $V_i = 1.75$, and thus if the feed volume had been <0.7 CV, the diffuse wave at the top of the trailing edge had run down the shock wave at the leading edge and eliminated the plateau of the feed pulse completely. In this example, the feed lasted 1 CV, and this means the shock wave left the column 0.3 CV before the top of the diffuse wave reached the column exit.

The elution volume of the shock wave at the leading edge of the elution profile is shown in Figure 2.8 as the vertical dashed–dotted line at 1.75 CV, and the elution profile of the trailing edge is depicted as the curved line starting at $V_i = 1.05 + 1$ CV and ending at $V_i = 7.34 + 1$ CV. The original plateau of 1 CV of the feed pulse was reduced to a plateau of 0.3 CV. The area encircled by the elution profile and the baseline is 5 mM·CV. The arrows connected with a dashed–dotted line indicate the distance between the front of the feed pulse and the resulting shock wave, and the arrows connected with a solid line indicate the rear of the feed pulse and the resulting trailing edge of the elution profile.

The second example is depicted in Figure 2.9. The feed concentration and the salt concentration are identical with the concentrations in the previous example. The feed pulse started at $V_i = 0$, and it lasted for half a column volume, that is, the load was 2.5 mM·CV. The feed pulse is shown as the dotted square function from 0 to 0.5 CV. In the first example, the shock wave generated at the front of the feed pulse made it to the column exit because the duration of the feed pulse was larger than 0.7 CV, but in the second example, the duration of the feed pulse was reduced to 0.5 CV. This means that the top of the diffuse wave ran down the shock wave before the column exit and that diminished the

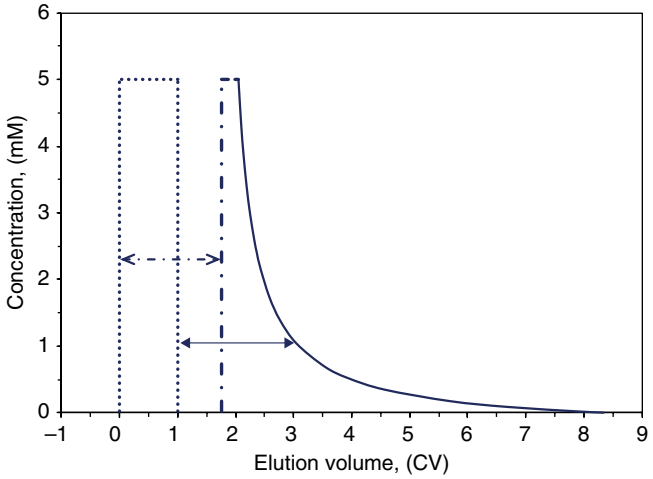

Figure 2.8 The ideal elution profile of a GLP-1 derivative on a Source 30 Q adsorbent with 0.03 M sodium chloride in the feed and in the eluant. The dotted square from 0 to 1 CV represents a load of 5 mM·CV. The front of the feed pulse enters at $V_i = 0$. The curved line is the trailing edge of the elution profile, and the vertical dashed–dotted line at $V_i = 1.75$ CV is the leading edge of the elution profile. The arrows connected with a dashed–dotted line indicate the distance between the front of the feed pulse and the resulting shock wave. The arrows connected with a solid line indicate the rear of the feed pulse and the resulting trailing edge of the elution profile.

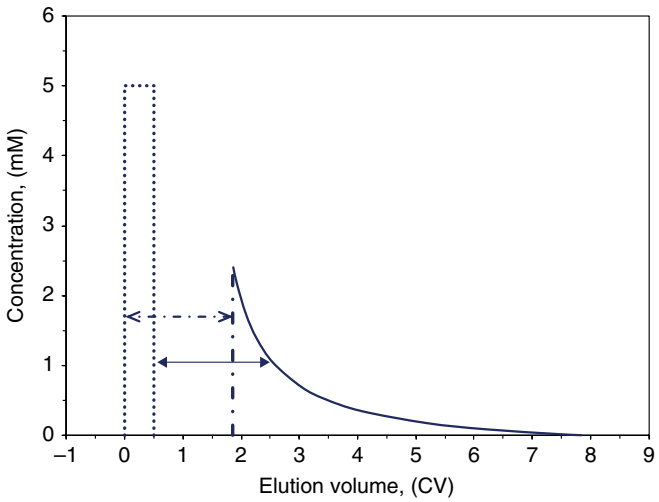

Figure 2.9 The ideal elution profile of a GLP-1 derivative on a Source 30 Q adsorbent with 0.03 M sodium chloride in the feed and in the eluant. The dotted square from 0 to 0.5 CV represents a load of 2.5 mM·CV. The front of the feed pulse enters at $V_i = 0$. The curved line is the trailing edge of the elution profile, and the vertical dashed–dotted line at $V_i = 1.86$ CV is the leading edge of the elution profile. The arrows connected with a dashed–dotted line indicate the distance between the front of the feed pulse and the resulting shock wave. The arrows connected with a solid line indicate the rear of the feed pulse and the resulting trailing edge of the elution profile.

concentration at the leading edge of the concentration profile in the column and slowed down the speed of the shock wave. The elution volume at the leading edge must therefore be determined from the material balance.

The elution profile at the trailing edge, resulting from a diffuse wave, is the full line ending at $V_i = 7.34 + 0.5$ CV. The position of the shock wave at the leading edge of the elution profile was determined by the fact that the area under the trailing edge of the elution profile from $V_i = 7.84$ CV to the leading edge of the elution profile must be equal to the area of the feed pulse, that is, 2.5 mM·CV. The material balance showed that the shock wave eluted at $V_i = 1.86$ CV. The leading edge is shown as the vertical dashed–dotted line at $V_i = 1.86$ CV on the figure. The arrows connected with a dashed–dotted line indicate the distance between the front of the feed pulse and the resulting shock wave. The arrows connected with a solid line indicate the rear of the feed pulse and the resulting trailing edge of the elution profile.

When comparing Figures 2.5, 2.8, and 2.9, it is easy to identify some very important similarities. The result of the analysis, the elution profiles shown in Figures 2.8 and 2.9, explains the curvature of the trailing edges observed in the simulated elution profiles and the steep leading edges as well. The simulations also account for the dispersion forces, and that explains why the leading edges in the simulated elution profiles are not vertical. In the calculations shown in Figures 2.8 and 2.9, the development of the leading edge of the elution profile, resulting from the step-up in the feed concentration, started at $V_i = 0$ CV, and the development of the trailing edge of the elution profile, resulting from the step-down in the feed concentration, started when the feed pulse ended at $V_i = 1$ and 0.5 CV, respectively. In a simulation, the load was focused in the column at low salt concentration at the column entrance before the elution started. This means that the development of the trailing edge of an elution profile started at $V_i = 0$ at all loads; wherefore all trailing edges of the elution profiles form a common envelope up to the inflection point on the trailing edge.

The trailing edge of the ideal elution profile is indicated in Figure 2.5 as the thin full line that extends above the plateau of the elution profiles. It is depicted with a minor horizontal displacement in order to make it coincide with the envelope of the trailing edges of the simulated elution profiles. There is a good agreement between the curvatures of the two profiles at concentrations up to 3 mM. The agreement will probably depend on the dispersion in the column.

2.7.1.4 Modeling the Trailing Edge of a Peak at High Load

The slope of the trailing edge of the ideal elution profile, $\partial V_i / \partial c$, is proportional to the second derivative of the adsorption isotherm. The analysis presented in Section 2.7.1.3 showed the similarity in the slope of the trailing edge of the ideal elution profile and the slope of the envelope of the trailing edges of the simulated elution profiles at high load. The comparison is depicted in Figure 2.5. This observation was utilized to calculate the second derivative of

the adsorption isotherm from the simulated data, and finally, the calculated values of the second derivative were used to estimate the maximum adsorption capacity. If the retrieved value of the maximum adsorption capacity is close to the model parameter, it shows that this approach can be utilized with some confidence when experimental data replace the simulated data.

In order to model the trailing edge of an elution profile at high load, the following approximations are used:

$$\begin{aligned} V_i(c) \simeq d + V_{\text{diffuse}} &= d + V_{NA,i} + (1-\varepsilon_{\text{b}})\varepsilon_{\text{p}} k_{d,i} \frac{\partial q}{\partial c} \\ &= d + V_{NA,i} + (1-\varepsilon_{\text{b}})\varepsilon_{\text{p}} k_{d,i} \frac{\partial F}{\partial c} \end{aligned} \tag{2.58}$$

where d is a horizontal displacement that accounts for the dispersion and $F(c)$ is a function utilized to fit the curvature of the trailing edge. It must have the property that $F'(0) = A_i$, and it must be applicable up to the inflection point where $\partial^2 V/\partial c^2 \leq 0$. A quadratic isotherm [1] is a suitable choice for $F(c)$:

$$F(c) = \frac{A_i c + ac^2}{1 + Bc + bc^2} \tag{2.59}$$

That is,

$$\frac{\partial F}{\partial c} = \frac{A_i + 2ac}{1 + Bc + bc^2} - \frac{\left(A_i c + ac^2\right)(B + 2bc)}{\left(1 + Bc + bc^2\right)^2} \tag{2.60}$$

and according to Equation 2.58

$$\frac{\partial^2 F}{\partial c^2} = \frac{\partial^2 q}{\partial c^2} \tag{2.61}$$

To test the hypothesis, the model, Equation 2.58, was fitted to the trailing edge of the elution profile at a load of 5 mM·CV in the interval $7.34 \geq V_i \geq 2$ CV, corresponding to a concentration interval of $0.03 \leq c_i \leq 3.6$ mM. The number 7.34 CV is the value of the ideal elution volume at $c_i = 0$, and at elution volumes <2 CV, the curvature of the elution profile changes. The fitted parameters, a, B, b, and d, are given in Table 2.2.

To test the validity of the approximation the residual sum of squares,

$$\text{RSSQ} = \sum \left(\frac{\partial^2 F}{\partial c^2} - \frac{\partial^2 q}{\partial c^2} \right)^2 \tag{2.62}$$

Table 2.2 Estimated parameters in $F(c)$, Equation 2.59.

A_i (mM^{-1})	a (mM^{-2})	B (mM^{-1})	b (mM^{-2})	d (CV)
20.98	25.5	3.21	0.946	0.64

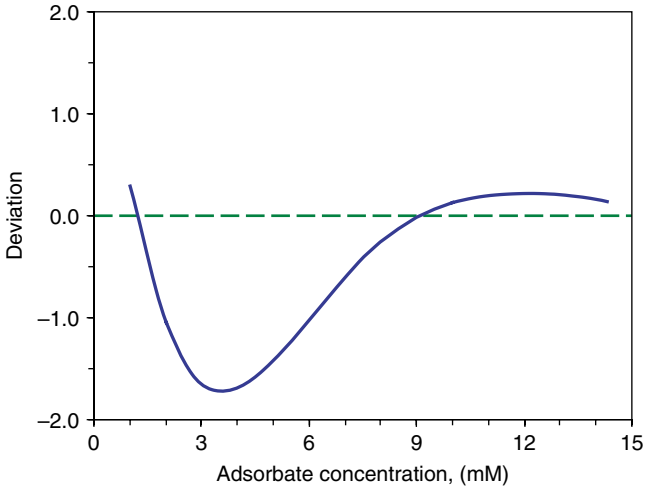

Figure 2.10 The solid line shows the deviation between the second derivative of the isotherm and the second derivative of the $F(c)$ function. Details are given in Section 2.7.1.4.

was minimized using 14 specified adsorption capacities from 1 to 14 mM at intervals of 1 mM by adjusting the maximum adsorption capacity. The corresponding solute concentrations ranged from 0.05 to 3.3 mM. The second derivative $\partial^2 q/\partial c^2$ was calculated from Equation 2.53. The estimated value of the maximum adsorption capacity was 39.5 mM, which is almost identical with the value used in the simulations, which was 39.16 mM. The deviation plot is shown in Figure 2.10.

As for any least square parameter estimation method, this method will be sensitive to the selected data interval. The influence of the load, the salt, and the solute concentrations in the feed has not been explored. A high load is most likely preferable. The influence of the dispersion on the reliability of the results was not investigated either.

2.8 Hydrophobic Adsorbents, HIC and RPC

Adsorbents in HIC are less hydrophobic than adsorbents in reversed-phase chromatography (RPC). The modulator in HIC is salt, and the adsorbate is eluted by reducing the salt concentration in the eluant. In RPC the modulator

is an organic water-soluble solvent, and the adsorbate is eluted by increasing the solvent concentration in the eluant.

The classical adsorption isotherm model is derived from Equation 2.52 when $\sigma = 0$:

$$\frac{q_i}{c_i} = \tilde{K}_i \tilde{\Gamma}_i \left(\frac{\Lambda}{c}\right)^{\nu_i} \left(1 - \sum_{j=1}^{\alpha} \frac{q_j}{q_j^{\max}}\right)^{\nu_i} \tag{2.63}$$

This adsorption isotherm has, like the corresponding ion exchange adsorption isotherm, a negative curvature, that is, the solute velocity increases with increasing concentration; wherefore a shock wave is formed at the leading edge of the elution profile, and a diffuse wave shapes the trailing edge of the elution profile. The excess potentials play a crucial role in the modeling in contrast to what is commonly observed in ion exchange chromatography. The excess potentials of macro-ions are functions of the nature and the concentrations of salt and solvents and of the temperature and pH. In Section 2.A.4, the Kirkwood theory of dipolar ions is analyzed, a theory that accounts for salting-in and salting-out potentials of macro-ions.

The initial slope of a classical hydrophobic adsorption isotherm is

$$A_i = \left(\frac{\Lambda}{c}\right)^{\nu_i} \tilde{K}_i \tilde{\Gamma}_i = \left(\frac{\Lambda}{c}\right)^{\nu_i} \exp\left(-\frac{\Delta G_i^0}{RT}\right) \tilde{\Gamma}_i = A_{0,i} \tilde{\Gamma}_i \tag{2.64}$$

Isocratic retention data measured on HIC adsorbents can be utilized to develop models of the equilibrium excess functions of the retained components. $A_{0,i}$ varies with the solvent concentration, and $\tilde{\Gamma}_i$ depends on the salt and solvent concentrations. When measuring reversed-phase retention data, it is thus essential to measure the retention data at constant solvent composition and vary the salt concentration because otherwise one cannot distinguish the variation of $A_{0,i}$ with the solvent composition from the variation of $\tilde{\Gamma}_i$ with the solvent composition.

The fundamental equation for the relative retention in HIC and RPC is

$$\ln R_i = \ln\left(1 - \varepsilon_b\right) \varepsilon_P k_{d,i} + \ln \tilde{K}_i + \nu_i \ln\left(\frac{\Lambda}{c}\right) + \ln \tilde{\Gamma}_i \tag{2.65}$$

where

$$RT \ln \tilde{\Gamma}_i = -\left(\overline{\tilde{\mu}}_i^E - \tilde{\mu}_i^E\right) \tag{2.66}$$

Since $\ln \tilde{\Gamma}_i$ is a function that accounts for the contributions of the excess potentials, it is common practice to depict the experimental values of $\ln R_i$

versus the salt concentration. The graph will show how $\ln \tilde{\Gamma}_i$ varies with the salt concentration at constant solvent composition, and in many cases, a linear dependence of the salt concentration can be observed. In HIC, it is common to observe salting out, and in RPC one often observes salting in.

In Section 2.8.1, an analysis of the modeling of the retention of lysozyme on the Toyopearl Butyl-650S, Phenyl-650S, and Toyopearl Ether-650S adsorbents is presented. In Section 2.8.2, the retention data of three insulin components measured on the Toyopearl Butyl-650S and Toyopearl Phenyl-650S adsorbents are analyzed and modeled. Finally, in Section 2.8.3 similarities and differences in the retention behavior of lysozyme and the insulin components are analyzed, and some preliminary conclusions are drawn.

2.8.1 The Adsorption of Lysozyme

The isocratic retention volumes of lysozyme were determined on the Toyopearl Butyl-650S, Phenyl-650S, and Ether-650S adsorbents, from Tosoh Bioscience at pH 7 [11]. These data were utilized to develop a model of the equilibrium excess function of the lysozyme component at infinite dilution. In order to develop a model that also accounts for the influence of the lysozyme concentration, the model was extended to include correlation of the solubility of lysozyme.

Figure 2.11 depicts the experimental and correlated isocratic retention volumes of lysozyme on Toyopearl Butyl-650S at pH 7 and the predicted retention

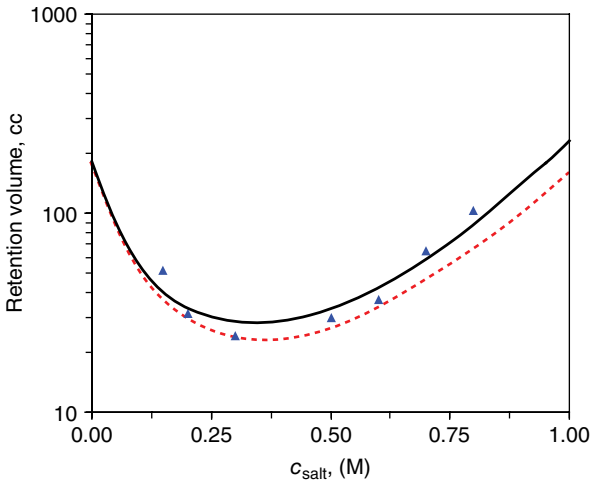

Figure 2.11 Experimental and modeled isocratic retention volumes of lysozyme on a Tosoh Butyl-650S adsorbent at pH 7 with ammonium sulfate in the eluant. The triangles show the experimental data, and the solid line shows the correlation. The dashed line is the predicted retention volume at pH 4.